Thermoplastic Microfluidics for 3D Cell Culturing

by

HATİCE NUR BAŞER

A Dissertation Submitted to the
Graduate School of Sciences and Engineering
in Partial Fulfillment of the Requirements for
the Degree of

Master of Science

in

Biomedical Science and Engineering

February 6, 2023

Thermoplastic Microfluidics for 3D Cell Culturing

Koç University

Graduate School of Sciences and Engineering

This is to certify that I have examined this copy of a master's thesis by

Hatice Nur Başer

and have found that it is complete and satisfactory in all respects,
and that any and all revisions required by the final
examining committee have been made.

Committee Members:

Prof. Dr. Alper Kiraz (Advisor)

Asst. Prof. Ahmet Can Erten [Co-Advisor]

Prof. Dr. Kemal Baysal

Asst. Prof. Berna Morova

Assoc. Prof. Onur Ferhanoğlu

Date: 06.02.2023

Dedicated to my family for all their support, love, and encouragement.

ABSTRACT

Thermoplastic Microfluidics for 3D Cell Culturing

Hatice Nur Başer

Master of Science in Biomedical Science and Engineering

February 6, 2023

Microfluidic platforms have recently become essential in cell studies since they can closely mimic the 3D cell culture environment. These platforms need to have hydrophilic, transparent, and biocompatible properties. Material selection, fabrication method, and bonding type are critical for biomedical studies to achieve these purposes. This thesis has focused on polydimethylsiloxane (PDMS)and polymethyl methacrylate (PMMA) as materials for the formation of microfluidic chips with unique physical and chemical properties.

The first part of the thesis focuses on PDMS chips produced by the soft lithography method and cell studies performed with these chips. In the second part, the leading research is based on the solvent bonding technique for forming PMMA chips. We did surface analyzes to investigate the quality of microfluidic platform building with thermoplastics. We found optimum parameters for temperature and solvent type for bonding PMMA microfluidics. The final version of this platform has allowed the creation of a functional environment for 3D cell culture work.

ÖZETÇE

3B Hücre Kültürü için Termoplastik Mikroakışkanlar

Hatice Nur Başer

Biyomedikal Bilimleri ve Mühendisliği, Yüksek Lisans

6 Şubat 2023

Mikroakışkan platformlar, 3D hücre kültürü ortamını yakından taklit edebildikleri için son zamanlarda hücre çalışmalarında alternatif bir metot haline geldi. Bu platformların hidrofilik, şeffaf ve biyouyumlu özelliklere sahip olması gerekir. Bu amaçlara ulaşmak için biyomedikal çalışmalarda kullanılacak malzeme seçimi, yapılacak üretim yöntemi ve bağlanma tipi kritik öneme sahiptir. Bu tezde, benzersiz fiziksel ve kimyasal özelliklere sahip termoplastik bir malzeme olan Polimetil Metakrilat (PMMA) ve siloksan lineer polidimetilsiloksan (PDMS) kullanıldı. Tezin ilk bölümü soft litografi yöntemi ile üretilen PDMS ile yapılan hücre çalışmalarına odaklanmaktadır. İkinci bölümde ise temel olarak PMMA için solvent ile yapıştırma tekniğine anlatılmaktadır. Termoplastiklerle mikroakışkan platform yapısının kalitesini araştırmak için gerekli analizleri yapıldı. PMMA mikroakışkanlarını bağlamak için sıcaklık ve solvent tipi için optimum parametreler bulundu. Bu platformun son hali 3 boyutlu hücre kültürü çalışması için işlevsel bir ortamın yaratılmasına olanak sağlamıştır.

ACKNOWLEDGEMENTS

This thesis is supported by the TUBITAK (The Scientific and Technological Research Council of Turkey) project numbered 119E138.

I want to thank to following people for their help and encouragement: especially my advisors, Prof. Dr. Alper Kiraz and Asst. Prof. Ahmet Can Erten. I also thank Prof. Dr. Kemal Baysal for guiding and motivating cell studies. I thank Asst. Prof. Berna Morova for her kindness, suggestions, support, and valuable advice.

I would like to express my gratitude to my coworkers Jhan Luke Okkabaz, Amir Mohammad Ketabchi, Nima Bavili, and Ekin Özgönül for being good friends and providing a creative research environment.

I would like to thank my boyfriend of my biggest supporter, for his help, for being with me all the time, and for the motivation he has given me with his positive energy.

I would also like to thank my cats, Leo and Lena, who have never left me alone, even when I was writing this thesis at night.

I would like to thank my friends and family who have always supported me and their love.

TABLE OF CONTENTS

1. LIST OF TABLES

2. LIST OF FIGURES

3. ABBREVIATIONS

PDMS	Polydimethylsiloxane
PMMA	Poly (methyl methacrylate)
IPA	Isopropyl alcohol
ACE	Acetone
ETOH	Ethanol

CHAPTER 1:

INTRODUCTION

1.1 Microfluidics for 3D Cell Culturing

With the development of semiconductor technology, microfluidics has been a research field in biology, medicine, and industrial applications for nearly a century. The purpose of microfluidic systems is to manipulate the fluids at micron levels and to investigate the dynamics of these fluids. Microfluidic systems have many benefits over traditional methods in biomedical science. Building microfluidics in micro-size helps the lowering the cost of the reagents. Microfluidics not only reduces the sample volume compared to traditional methods but also allows the measurement of small volumes of these samples [Sackmann et al.,2014]. Thank these advantages, microfluidics technology has become a step between in vivo and in vitro experiments for biomedical studies since creating and managing complex structures is possible. Using Petri dishes for in vitro experiments causes problems. Firstly, controlling the chemical gradient of products such as oxygen and nutrients required for the cell is limited due to 2D culturing. In the real world, the cell constantly performs the vital functions necessary for itself, which means that this gradient happens automatically. The first goal of creating the microfluidics system for cell culturing is to mimic the natural environment. So, mimicking does not occur in Petri dishes. The second problem of 2D cell culture is that it has no sufficient medium to investigate multifunctional events such as cell migration, cell morphology, and protein expression since there is no 3-dimensional environment. [Elliott and Yuan, 2011, as cited in Li et al., 2012]

Microfluidics technology allows 3D cell studies thanks to its many benefits. Firstly, microfluidic technology allows for micro-scale designs, and this size is very close natural cell environment. It is a low-cost technology since the amount of material used in experiments at the micro level will be less. Unlike 2D cell culture, it is suitable for creating multidimensional cell culture media. In addition, it allows different cell experiments, such as cell capture and fluid control in the same environment. Also, the

materials used in producing microfluidic systems provide an advantage for cells by oxygen permeability [Li et al., 2012].

Therefore, researchers use microfluidics technology to get more reliable and low-cost methods for single-cell analysis, genetic assays, intracellular signaling, multidrug resistance, drug toxicity, pathogen detection, cell culture, and tissue engineering [Hosic et al., 2015; Spurgeon et al., 2008; Xu et al., 2013; Li et al., 2016; Theobald et al., 2017; Nguyen et al., 2019; Lei et al., 2017; Karimi et al., 2016].

1.2 Fabrication and Bonding Techniques in Microfluidics

Material selection, the production method of mold, and the bonding technique are the main parts of building a microfluidics platform. The materials currently used in microfluidics systems are divided into inorganic, polymers, and paper. Silicon, glass, and ceramic are inorganic materials, and silicon is the oldest material used for microfluidics [Terry et al.,1979; Roy et al., 2016]. Silicon is used mainly in electronic systems that require high resolution, and the lack of transparency in the visible region is a significant limitation in the imaging processes of biological systems. The solution to this problem is designing a hybrid system by covering the surface with a transparent material. However, a hybrid system requires additional processes for a cell application, which creates problems in fabrication. While silicon is an essential material in point-of-care devices, this priority is different in cell research of microfluidics. Secondly, glass is a transparent material that is highly resistant to high temperatures and aggressive liquids. The processing of glass is by low-cost methods such as UV photolithography and chemical etching. Due to its high hardness and low tensile strength, surface distortions may occur when processing glass with micro milling. Low-temperature co-fired ceramic (LTCC) technology, a low-cost technique compared to silicon and glass production methods, provides a very homogeneous surface. Since it is a multi-plating technique, obtaining a suitable system for cell culture studies is impossible. In addition, since ceramic is not a transparent material, it is unsuitable for biomedical imaging [Roy et al., 2016]. Paper-based microfluidic platforms are fabricated in two ways: lithographic and printing which have the cheapest cost compared to other materials [Liu and Crooks, 2011; Roy et al., 2016]. The system has two central parts in paper-based microfluidic systems: hydrophobic parts that act as barriers and hydrophilic parts used as open channels [Cateet

al., 2014]. Since these platforms are not transparent, imaging cannot be done, and they are unsuitable for applications requiring open channels. It is impractical to collect products because the paper is absorbent [Nishat et al., 2021].

Thanks to their unique properties, PDMS and thermoplastic materials are the most widely used materials in polymer microfluidics. PDMS is an elastomer material frequently used in cell-based studies [Halldorsson et al., 2015]. It has high gas permittivity with optical transmissivity. PDMS is fabricated by soft lithography, a straightforward method [McDonald et al., 2000; Torino et al., 2018 as cited in Shakeri et al., 2021]. PDMS consists of -OSi $(CH_3)_2$- group and is a hydrophobic material because of the CH_3 groups in its structure. This causes undesirable adsorption and considerably reduces wettability. Air plasma can be applied to make the PDMS hydrophilic. Si-OH groups are formed on the surface after plasma, increasing hydrophilicity. The hydrophilic property of PDMS gradually returns to its steady state after contact with air. Plasma treatment is also a method used for bonding PDMS. Plasma is applied to the surface to be bonded with PDMS; in this way, Si and O are bonded with covalent bonds on both surfaces [Sia and Whitesides, 2003]. There are studies in the literature in which cell studies are carried out using PDMS-based microfluidic chips [Tanyeri and Tay, 2018]. In another PDMS-based microfluidic platform, in which the mold prepared by 3D printing was used, the gradient of human cells under the influence of many different chemicals was examined [Kamei et al., 2015]. Despite its advantages, solvent swelling, hydrophobic molecule absorption, lack of mechanical rigidity, or low fabrication throughput significantly limit PDMS in biomedical research. PDMS generally contributes to research in situations that allow rapid prototyping in the laboratory environment but are unsuitable for mass production [Halldorsson et al., 2015; Lee et al., 2003, as cited in Giri and Tsao,2022]. The most used thermoplastics in microfluidics are poly (methyl methacrylate) (PMMA), polycarbonate (PC), polystyrene (PS), and cyclic olefin polymer/copolymer (COC/COP). They show good mechanical rigidity, organic solvent resistivity, acid/base resistivity, and low water absorption. Table 1.1 shows these thermoplastic materials' physical, chemical, and optical properties. As seen from the table, the melting temperature of PMMA is around 104°, and it is highly resistant to solvents such as acid-base. In addition to these features, PMMA is one of the most frequently used transparent materials in microfluidics in cell studies since its optical transmittance is quite good in the UV and visible regions [Bangslabs,2022; Roth and

Drummer 2021 as cited in Giri and Tsao,2022]. In a study, microfluidic platforms for mimicking the human blood vessel wall in vitro smooth muscle cells (SMCs) and human umbilical vein endothelial cells (HUVECs) were used, in which PMMA bonded with Poly (acrylic acid) via UV was used. It shows PMMA is a good alternative for mimicking the cell environment [Le et al., 2021].

Table 1.1: Physical, chemical, and optical properties of thermoplastics [Giri and Tsao,2022].

Thermoplastic Materials	Physical Properties				Chemical Resistance		Optical Transmissivity		Reference
	Young's Modulus	T_g [1]	T_m [2]	CTE [3]	Solvent	Acid/Base	Visible	UV	
Polymethylmethacrylate (PMMA)	3200	104–105	130	6–8	good	good	excellent	good	[13]
Polystyrene (PS)	2300–4100	80–90	240–260	10–150	fair	good	excellent	fair	[13]
Cyclic olefin polymers (COC/COP)	2600–3200	65–170	190–320	60–80	excellent	good	excellent	excellent	[14]
Polycarbonate (PC)	2300–2700	145–148	260–270	60–70	good	good	excellent	fair	[15]

After selecting a suitable material for cell culture studies to use in the microfluidic platform, two steps remain to build a microfluidics platform. These steps are forming the microchannel geometry and then bonding the materials. Choosing a fabrication and bonding method suitable for the material is critical for the microfluidics platform. This section will discuss fabrication and bonding techniques used in the literature for thermoplastic materials. Hot embossing is a widely used method for shaping channels and bonding materials. By using high pressure and temperature, the thermoplastic material is shaped through the master mold and left to cool by continuing to apply pressure on it. During this process, the material sometimes cracks due to high temperature and pressure, and annealing can be done before the process to prevent this problem. Although hot embossing enables complex designs to be processed, having a medium cost and good surface finish, it has some limitations. The disadvantages of this technique are the need for a master mold, the lack of a high production rate, the occurrence of breaks during the process, and the difficulties in forming channels with high aspect ratios. Injection molding is another method used for processing thermoplastic materials. First, the polymer is melted above the glass transition temperature (Tg) and injected correctly into the master mold. After filling the master mold, it waits until the material cools down. The cooling process takes time compared to other processes. One of the solutions to shorten the cooling process is conformal cooling. Although this method offers a rapid process with

tight tolerances and high reproducibility, the cost of equipment, the need for a master mold, and the inability to make channels with large footprints are the limitations [Jena&Yue, 2012; Su et al., 2019 as cited in Shakeri et al., 2022]. Another fabrication method with a lower cost than the injection molding is laser ablation. After coating the thermoplastic material with a photoresist in the desired geometry, it takes its final shape employing a laser. To do laser ablation, it is essential to have a cleanroom. This process provides much flexibility in changing the design since no master mold is needed. However, surface quality decreases after laser ablation. Also, this method does not allow complex designs and causes bulge formation [Attia et al., 2009, as cited in Shakeri et al., 2022]. Another low-cost method used for microchannel forming is micro-milling. This method contains fewer parameters than other methods. There is no waste of time in finding the optimum value of parameters such as temperature and pressure because it is independent of these parameters. The first step is to draw the design in a drawing program, which is an easy technique that requires pressing the machine's button. Micro milling not only provides flexibility in modifying the design as desired without the need for any master mold or a photoresist material but also allows the forming of complex designs [Bruijns et al., 2019, as cited in Shakeri et al., 2022]. The size limit of the micro-milling technique is a width of fewer than 30 micrometers and a surface roughness of one-tenth of a nanometer. As mentioned, it allows commercializing microfluidic platforms due to its flexibility in geometry modification and rapid prototype [Xue et al., 2020].

Bonding is the third and final step in microfluidics platform development. The critical parameters for bonding microfluidic chips used in cell studies are listed as follows: bonding strength is as high as possible, optical clarity is not adversely affected after bonding and biocompatibility. Since thermoplastic materials used for microfluidics studies generally have similar physical or chemical properties, there are many different techniques for bonding these materials. These methods are thermal bonding, solvent bonding, and adhesive bonding. Thermal bonding is a technique of bonding different or the same thermoplastic materials; a hot press is needed since it requires high temperature and pressure. Determining optimum temperature, pressure, and waiting times according to the material is critical. High temperature and pressure cause the channels to deform or even close, while too low temperature and pressure cause no bonding. In this technique, the bonding temperature is close to the melting point of the thermoplastic material, so the thermoplastic material may break while cooling after bonding. The solution for this

problem is surface modification before bonding. [Tsao and DeVoe, 2009; Lai et al., 2004; Kelly and Woolley, 2003 as cited in Trinh., 2022]. In literature, some studies imply surface treatments such as plasma and UV increase the bonding strength while lowering the temperature required for bonding [Mekaru, 2018; Liu et al., 2009, as cited in Trinh, 2022].

The second bonding type is adhesive bonding, a process of bonding different thermoplastics with an adhesive material in a very cheap and straightforward method. In adhesive materials that are liquid and dry, the liquid adhesive needs extra stimuli: such as temperature or light. The requirement for dry adhesive material is the application of pressure. Although it is cheap and easy to make, the biggest problem with this technique is the clogging of the channels due to the excessive use of adhesive material [Chen et al., 2016, as cited in Trinh, 2022]. Among all bonding types, solvent bonding is the easiest to apply and is low-cost because it does not require costly equipment. The purpose of this bonding method is to break the bonds of thermoplastic materials by using solvent and then to form a microfluidic chip by bonding the exposed bonds with the evaporated solvent. The parameters to be considered in solvent bonding can be listed as follows: temperature, pressure type and amount, solvent type and amount, and bonding time. If the concentration of the solvent used increases, the bonding strength also increases. In addition, the optimum temperature is less than the melting temperature of the thermoplastic material; otherwise, deformations will occur. Clogging of channels encountered in other bonding types is no longer a problem for solvent bonding when the optimum temperature, pressure, and appropriate solvent type and amount are available. In the next section, important parameters affecting solvent bonding will be discussed. [Trinh et al., 2021]

1.3 Solvent Bonding in Microfluidics

Finding a suitable solvent for the thermoplastic material to be used for research in solvent bonding technique is one of the most critical steps. Hildebrandt parameter determines the type of solvent for the bonding of thermoplastic material. The equation of this parameter is as follows.

$$\delta = \left[\frac{(\Delta H° - RT)}{v}\right]^{\frac{1}{2}} \quad (1)$$

In equation 1, ΔH° refers to the difference between the latent heat of vaporization, R is the gas constant, T is the absolute temperature, v is the cohesive energy density, and δ is the Hildebrandt parameter. As seen from the equation, the Hildebrandt parameter gives information about the cohesive molecular force's calculation [Hildebrandt and Scott 1949 as cited in Tsao and DeVoe, 2008]. Investigating this calculation applied for the solvent and the solute makes it predictable whether bonding will occur. If Hildebrandt parameters of the solvent and material are close, the microchannels will likely be completely clogged. Similarly, bonding does not occur if the Hildebrandt parameters of two materials are too far apart. When selecting the appropriate solvent for thermoplastic materials, the Hildebrandt parameter should be too close nor too far. Table 1.2 shows Hildebrandt values of some thermoplastic materials and solvents [Brydson 1999, as cited in Tsao and DeVoe, 2008].

Table 1.2: Hildebrandt solubility parameters for thermoplastic polymers and organic solvents. [Brydson 1999; Barton 1991; Fitzpatrick and Dean 2002 as cited in Tsao and DeVoe, 2008]

Thermoplastic	δ [(J/cm^3)$^{1/2}$]
PTFE	12.6
PE	16.3
PP	16.3
COC	17.7
PMMA	20.1
PS	18.7
PVC	19.4
PC	19.4
PET	21.8
Solvent	**δ [(J/cm^3)$^{1/2}$]**
Cyclohexane	16.7
Methylene dichloride	19.8
Ethylene dichloride	20.0
Acetone	20.4
n-Hexanol	21.8
Isopropanol	23.4
Acetonitrile	25.1
Ethanol	26.0
Dimethyl sulfoxide	26.7
Methanol	29.6
Water	47.7

As given in Table 1.2, the solubility parameter is 20.1 $(J/cm^3)^{1/2}$ for PMMA and 20.4 $(J/cm^3)^{1/2}$ for acetone. If PMMA material is bonded with acetone, clogging problems in the channels is highly likely. To find the optimum solubility parameter, different percentages of different liquids or diluting solvents using deionized water needs

to be mixed [Tsao and DeVoe, 2008]. In a study using PMMA as a thermoplastic material, they did bonding coverage experiments at different solvent concentrations and temperatures. They used different concentrations of acetone and ethanol, and the system used an oven, microwave, and room temperature for heating. They found that the best scenario for bonding coverage is using high-concentration acetone and ethanol solutions and giving the temperature via microwave. However, according to the microscope images of these microfluidic chips' cross-sections, there appears to be a blockage in the channels of the microfluidic chips with solvents prepared at very high concentrations [Tsao et al., 2022]. Therefore, bonding strength and coverage are essential characteristics when finding the optimum scenario. In another study, four different mixtures according to the Hildebrandt parameter were used for bonding PMMA to PMMA. They investigated bonding strength, coverage, and burst tests to find a high-quality bonding scenario. Unlike other studies, plasma treatment was applied to PMMA material as a surface modification before bonding. The results showed that the bonding strength increased in all the microfluidic chips obtained by applying plasma [Faghih and Sharp, 2019]. Also, there is another method for getting high-quality bonding for PMMA. Retention grooves around the design and PMMA edges can be added to increase bonding coverage. Since the solvents used are volatile, the retention grooves add the system for improving the bonding coverage [Wan et al., 2017]. In a study, they used ethanol for bonding PMMA to PMMA, PET, and PC by using spin coating for homogeneous coating. In the final stage, UV provided bonding for these thermoplastic materials. Afterward, they found that the PMMA-PMMA bonding did not leak, and the channels were not deformed. As a result, materials with the same surface chemistry have better bonding [Chen and Duong, 2016].

1.4 Thesis Organization

The organization of this thesis is as follows: In chapter 2, the fabrication of PDMS-based microfluidic chips for cell culture formation will be mentioned. The molds obtained by cutting tapes of different heights with a digital craft cutter and the production of molds obtained from candles processed with CNC will be explained. The results of cell culture studies with these chips will be mentioned. In Chapter 3, among the solvent mixtures formed with different concentrations of IPA and ACE, the bonding scenario, which has the highest bonding strength and is most suitable for cell studies, will be discussed to

bond PMMA where the formation of microchannels with micro milling. In this study, solvent type, time, temperature, and plasma are among the parameters. In addition, the retention groove's effect on bonding quality will be discussed. The results of the experiments in Chapter 2 and Chapter 3 will be summarized in Chapter 4.

Chapter 2

PDMS-BASED MICROFLUIDIC CHIPS FOR 3D CELL CULTURING

2.1 Microfluidic Chip Design for 3D Cell Culturing

This study used a microfluidic chip design with a 3-channel structure, frequently used in the literature, especially in cancer-related studies such as angiogenesis [Wang et al., 2018]. The central channel is filled with hydrogel in the design that allows mimicking angiogenesis. Cells are seeded from one of the side channels. They are expected to diffuse into the hydrogel in the central channel due to the height difference between the central and side channels. After this stage, the microfluidics system is ready for chemical stimulus. In order to examine the factors affecting angiogenesis, chemical stimuli are given from the side channel that is not used for cell seeding. In further studies, grooves are added to the design for a place to generate tumor spheroids. The 2D AutoCAD drawings of three different designs are given in Figure 2.1.

The microfluidic chip designs in Figure 2.1 are suitable for rapid prototyping and mass production, easy to adapt to similar applications. The formation of the structure is as follows: a side channel width of 1 mm, a central channel width of 3 mm, and added to the main channel inlets 4 mm chambers. The height of the channels is 50 µm and 200 µm for the central and side channels, respectively. To minimize operator-related errors and to provide more repeatable fillings during the manual filling process, it was aimed to open the channel inlets larger than the micropipette tip and thus perform the channel fillings at ambient pressure. For this reason, 2.5 mm biopsy punches were used for the middle channel entrances and exits.

This study aims to form spheroids in grooves. Grooves are the form of recesses to be opened on the side surface of the hydrogel in the central channel. The cell-water mixture is filled into the side channel where the grooves are located. Next, the microfluidic chip is turned on for the cells heavier than water to drop to the bottom and fill the grooves. After the cells drop, there is a cleaning step for the side channel. Feeding liquid is used for sweeping the excess cells in the side channel without affecting the cells in the grooves. Flow volume is shown in Figure 2.2. It aimed to have designs where cells are not affected during cleaning, and there is no problem filling. For this purpose, two designs with different groove numbers and diameters are shown in Figure 2.1.

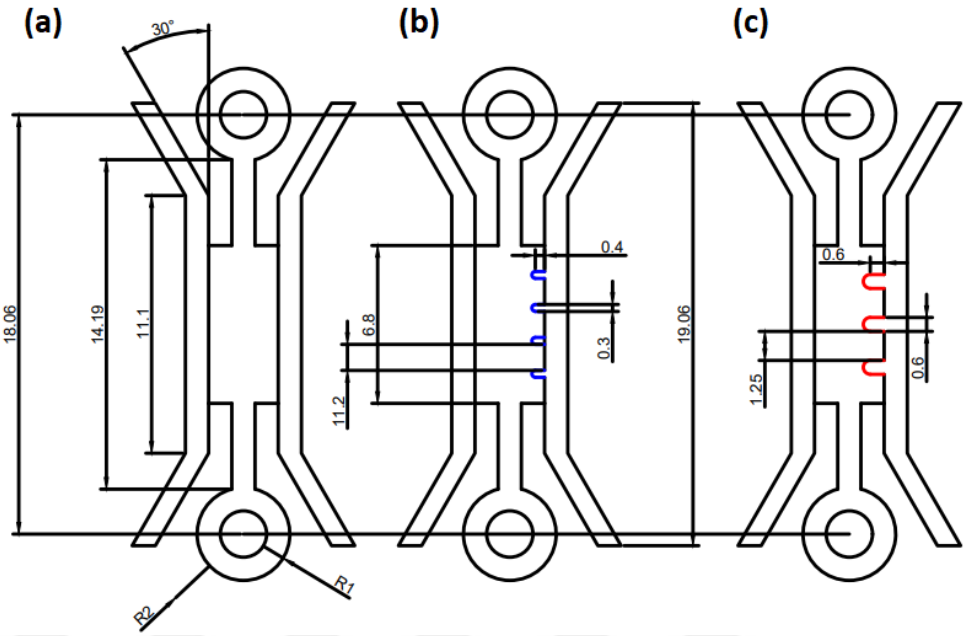

Figure 2.1: Two-dimensional drawing (mm) of the microfluidic chip (a) standard and (b) with 4 grooves design c) with 3 grooves design.

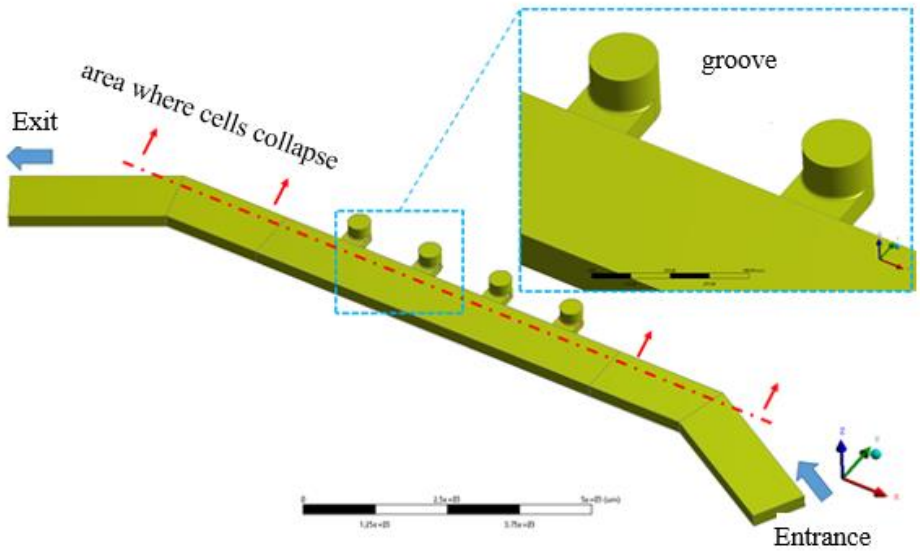

Figure 2.2: Flow volume in the first side channel design with grooves added.

In this chapter, PDMS-based microfluidic chips were investigated for different cell applications.

2.2 Materials and Method

In chapter 2, PDMS fabricated by soft-lithography technique was bonded to pdl coated glass (PDLcG; Menzel Glaser Polysine slides, Thermo Scientific). Momentive RTV615 branded PDMS was used at a ratio of 10:1. The mold was produced with a digital craft cutter (Silhouette Cameo, Silhouette America Inc.) by using adhesive polyimide (Kapton, 50 µm) and aluminum tapes (150 µm) that have different heights of the channels. Dektak, Bruker Corp was used for height profile analysis. For the confinement tests, Rhodamine B was prepared in deionized water with a concentration of 1 mM. The setup used for contact angle measurements is given in Figure 2.3. All contact angle measurements were made with the static sessile drop method with the setup shown in Figure 2.3. Each drop has a volume of 3 µl, and the CMOS camera acquired images. Contact angle measurement was done through images using the contact angle tool in the Image-j program. The cells within the microfluidic chip were imaged using an inverted confocal microscope (Leica DMi8 SP8) with a 10X objective.

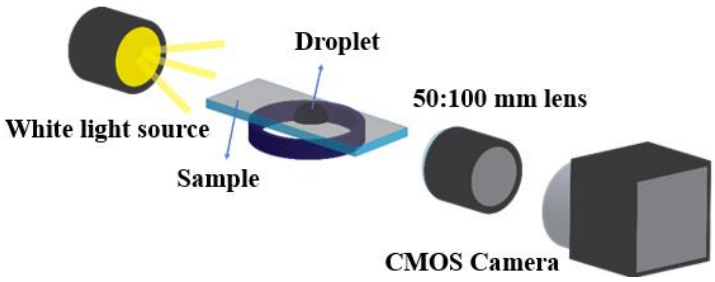

Figure 2.3: Schematic representation of the contact angle measuring setup.

2.3 Microfluidic Chip Fabrication

2.3.1 Preparation of molds

For the design pattern where the central channel height is 50 µm, and the side channel height is 200 µm, Kapton tape has adhered to acetate paper. After the drawing was saved as an AutoCAD file was opened in the Silhouette Studio, the device was started. Next, the aluminum tape was attached and machined to be on the side channels only. The images of the post-cut tapes are shown in Figure 2.4 [Coskun et al., 2022].

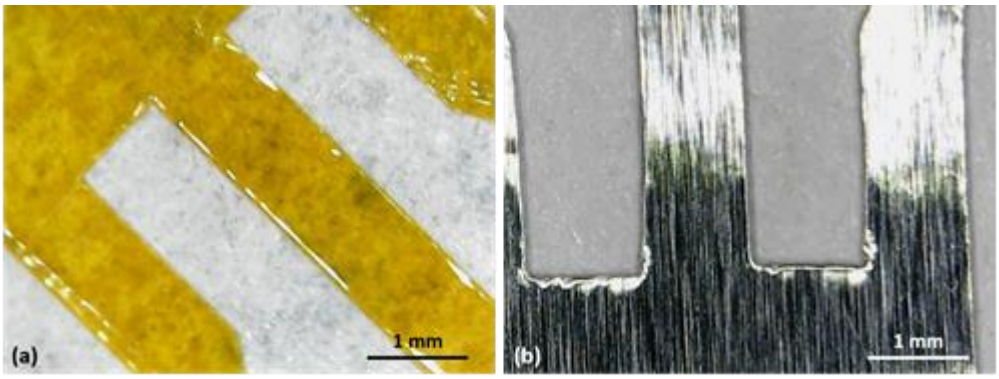

Figure 2.4: Images of tapes after cutting with a Silhouette craft cutter. (a) Kapton (b) Aluminum [Coskun et al., 2022].

The finished mold was placed on the plastic well plate using double-sided tape. Figure 2.5 is the schematic representation of the materials used in mold production. The top and bottom view of the mold placed on the plastic well plate is given in Figure 2.6 [Coskun et al., 2022].

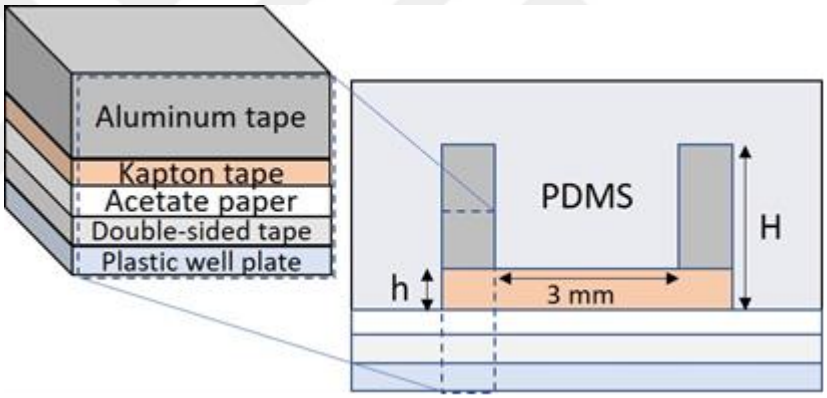

Figure 2.5: Schematic representation of the mold by layer [Coskun et al., 2022].

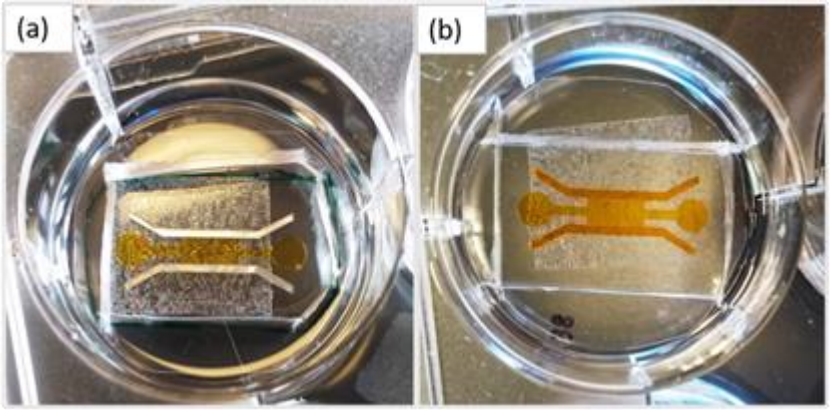

Figure 2.6: Different molds (a) The bottom layer with Kapton tape and the top layer with Aluminum tape; (b) The bottom and the top layers with Kapton tape [Coskun et al., 2022].

As the second method of mold production, wax was used for the PDMS microfluidic chips, as shown in Figures 2.7b and 2.7c. The patterns of these waxes were processed using CNC. The grooves in the design in Figure 2.7c have a width of 300 microns, and since these grooves are too small to be processed with a digital craft cutter device, all the designs that require grooves in this study were made by machining the mold wax with CNC.

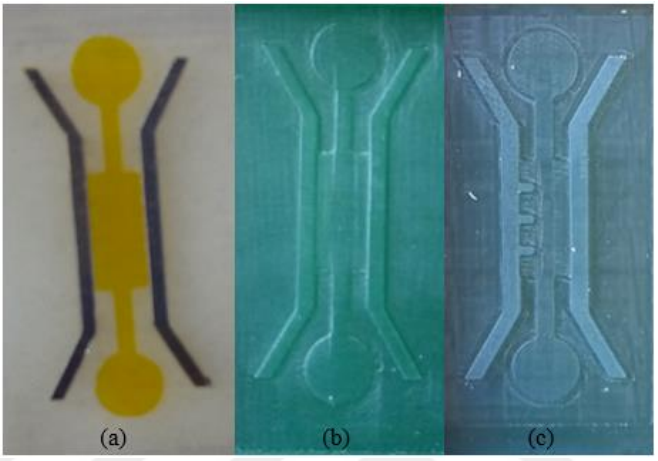

Figure 2.7: Photographs of the molds for PDMS microfluidic chip a) made of tapes having 50/200 µm height, b) wax mold having 150/400 µm, c) wax mold having 150/400 µm with three grooves.

2.3.2 Bonding of chips

PDMS was prepared 10:1 ratio. It was poured into the molds were kept in the oven at 65°C for 2 hours. After the PDMS was cured, it was removed from the mold using a razor. Inlets were drilled with biopsy punches with 1.5 mm and 2 mm core size diameters. For bonding of PDL-coated glass and PDMS, surface activation was performed with 60 seconds of oxygen plasma having 150 W radiofrequency (RF) power under a vacuum. PDMS was bonded to PDL-coated glass immediately after plasma treatment. Since the surface became highly hydrophilic after plasma, the microfluidic chip was heated in a 65-degree oven for 1 hour for hydrophobic recovery.

2.3.3 3D Cell Culturing

After the oxygen plasma treatment, microfluidic chips were sterilized under UV light in the laminar fluid cabin before use in cell culture studies.

The central channel was filled with a collagen solution which became a hydrogel following incubation at physiological pH and 37°C. First, the chemicals for hydrogel preparation listed in Table 3 were taken to an ice box in the laminar flow cabin and kept here for the experiment. Then, 1X DMEM, 10X Dulbecco's Modified Eagle's Medium

(DMEM, F-12 Ham with 15 mM HEPES and sodium bicarbonate, without L-glutamine, Sigma-Aldrich Inc), $NaHCO_3$ (7.5% w/v, sodium bicarbonate, Sigma-Aldrich), NaOH(1 M, sodium hydroxide, Sigma-Aldrich), and collagen(Type-I, bovine, 6 mg/mL, Sigma Aldrich Inc.) were mixed thoroughly in an Eppendorf tube on ice. In this recipe, the final collagen concentration was calculated as 2.98 mg/ml. It is crucial to mix the ingredients homogeneously during pipetting and not to form bubbles. Then, collagen was carefully added to the central channel. After loading collagen, the chips were placed in sterile Petri dishes, and then for the gelation of the hydrogen, they were incubated for 1 hour in a 37 °C incubator containing 5 %CO_2.

After the incubation, the leakage of the collagen in the channels was tested by using Trypan blue. For this test, 10 µL Trypan blue was loaded on the side channels and observed microscopically for 15-20 minutes. The microfluidic chips that pass the confinement tests are selected for cell studies. The side channels of the microfluidic chips were washed with PBS until the dye was removed [Coskun et al., 2022].

Table 2.1: Reagent volumes for preparing collagen [Coskun et al., 2022].

reagents	volume
10X DMEM	5 μL
NaOH 1M	0.5 μL
$NaHCO_3$ (7.5% w/v)	5 μL
1X DMEM	30 μL
collagen Type I (6 mg/mL)	40 μL

Cells such as endothelial and smooth muscle cells were added to the side channel and the cells were allowed to attach to the side surface of the collagen hydrogel. Following the adherence and growth of cells, they are fixed for further staining and imaging.

For fixation, the side channels were washed three times with 10 µL of PBS. Then, 3x10 µL of 10% paraformaldehyde solution was added to the channels, and the chips were put back into Petri dishes and stored at +4 °C until staining. Dyeing was done by following the steps. The side channels were washed four times with 10 µL of PBS. Then, 3x10 µL of phosphate buffer (PBS) solution containing 3% BSA + 0.1% Triton X-100 was added to the side channels and kept for 10 min at room temperature. The channels were washed four times with 10 µL of PBS. Then, 3x10 µL of 1% BSA solution prepared

in PBS was added to the channels and incubated for 1 hour at room temperature. The channels were washed four times with 10 µL of PBS. 10 µL of 1% Alexa Fluor 488 Phalloidin solution prepared in PBS was added to the side channel, then placed in Petri dishes incubated overnight at 37 °C. Distilled water or PBS was placed in Petri dishes to reduce evaporation. After incubation, the channels were washed with 10 µL of PBS four times. After adding 10 µL of DAPI (DAPI with Fluoroshield, Abcam) to both channels to mark the nuclei, the microfluidic chips were placed in Petri dishes in an opaque box and stored at +4 °C until imaging. Labeled microfluidic chips were viewed under the Leica DMi8 confocal microscope at the KUTTAM Imaging Center [Coskun et al., 2022].

2.4 Results

2.4.1 Profilometer Measurements

Channel profiles were measured with a Dektak profilometer over the mold made of Kapton and Aluminum tapes. The mold surfaces were scanned with a 12.5 µm stylus radius and 3 mg Stylus force for a length of 10000 µm and a 60 s. Profilometer result proves that the central (h=50µm) and side channel (H=200 µm) heights were obtained successfully. The Profilometer result of the mold is given in Figure 2.8.

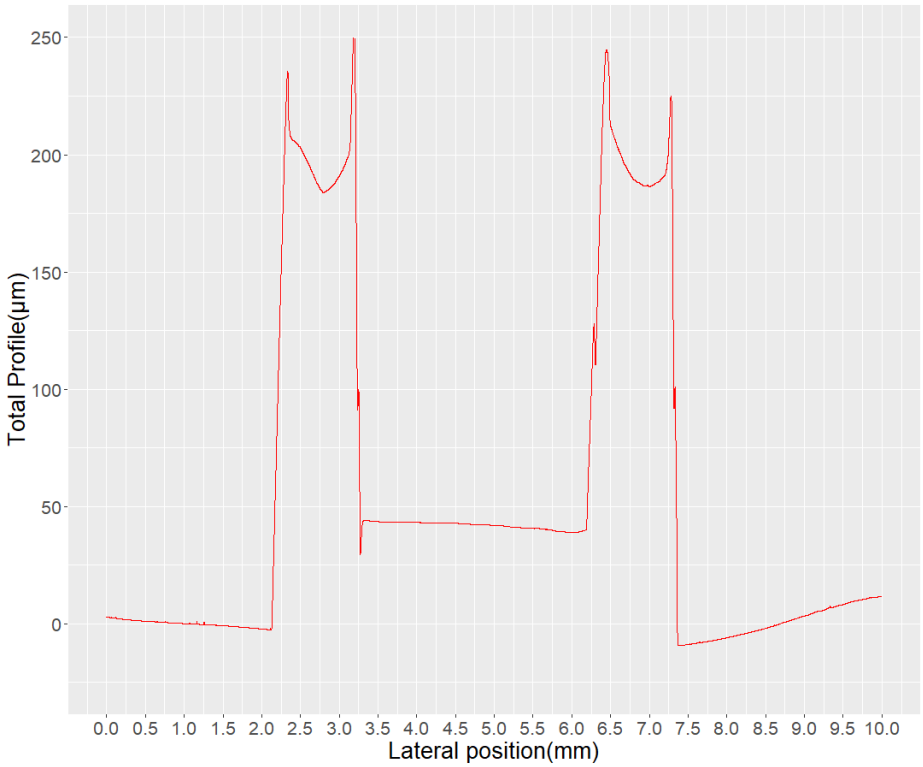

Figure 2.8: Profilometer analysis of mold having 50/200 µm height.

Profilometer analysis of the mold made of wax is given in Figure 2.10 with different directions. Figure 2.9 shows the direction of these profilometer measurements.

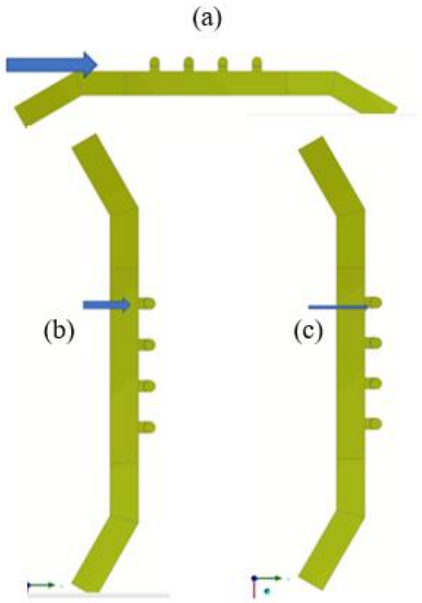

Figure 2.9: Different profilometer directions.

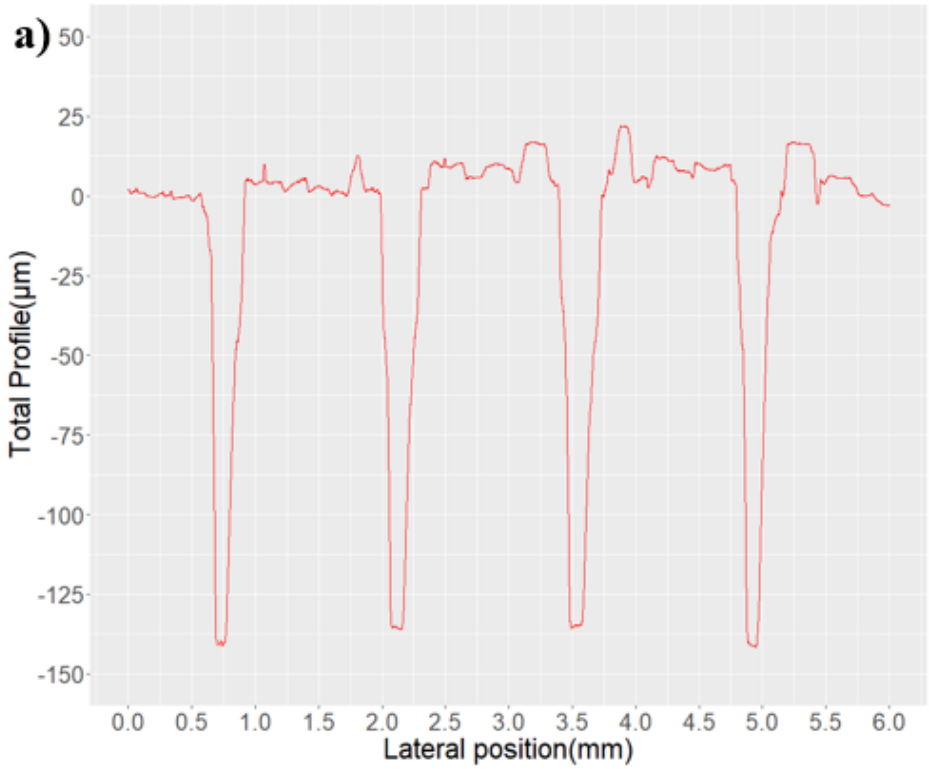

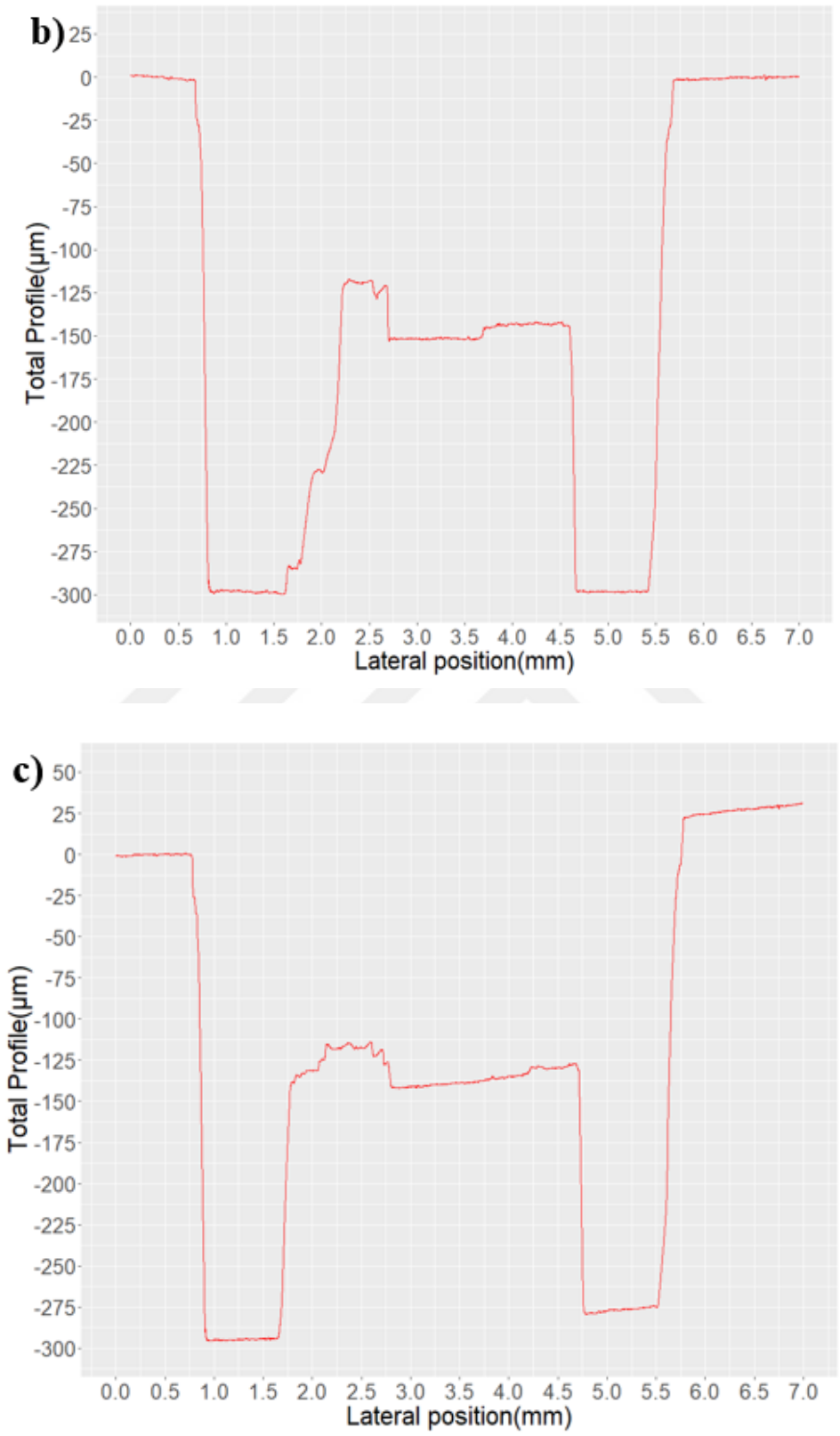

Figure 2.10: Profilometer measurements in different directions of the groove with h=150/400 µm heights and d=300 µm diameter width groove. a), b), and c) corresponding to Figure 2.9.

Based on the profilometer measurements in Figure 2.8, it has been proven to create designs at desired channel heights when using the wax mold.

2.4.2 Confinement Tests

Contact angle measurements analyze the wettability of the surfaces. The contact angles of deionized water and collagen were measured for PDMS, PDMS demolded over Kapton, Plain-glass, and PDL-coated glass. The images of the droplets are shown in Figure 2.11. Contact angle values of different surfaces are given in Table 2.2 [Coskun et al., 2022].

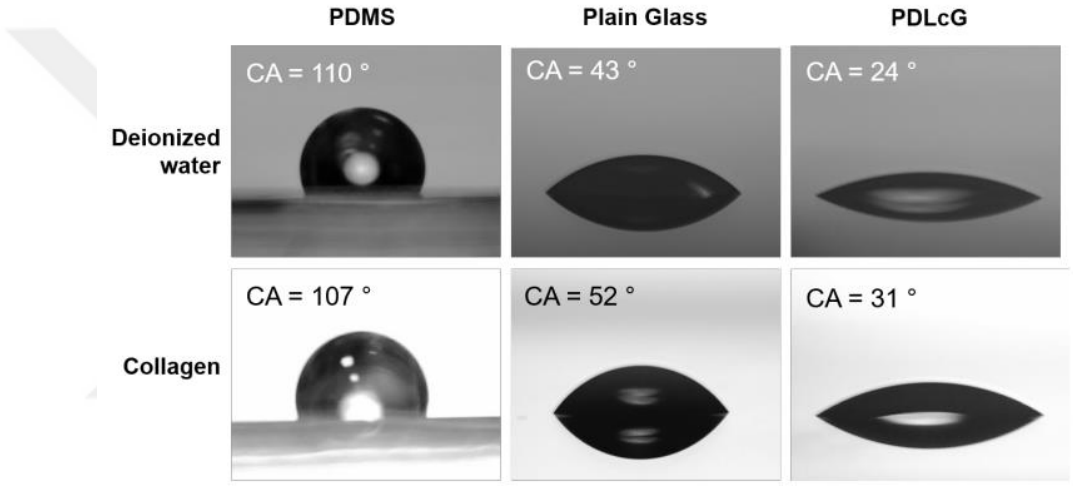

Figure 2.11: Images of different droplets with different surfaces [Coskun et al., 2022].

The contact angle of deionized water and collagen was almost the same for all surfaces. The highest contact angle was found for PDMS as it is hydrophobic. Contact angle values on PDL-coated glass were considerably lower than those on other surfaces. Due to its hydrophilic property, PDMS was bonded on PDL-coated glass in the study.

Table 2.2: Contact angles of water and collagen obtained on PDMS, glass, and PDL-coated glass [Coskun et al., 2022].

Surface	DI Water	Collagen
PDMS	110 °	107 °
PDMS demolded over Kapton	111°	-
Glass	43 °	52 °
PDL-coated glass	24 °	31 °

The study used water as the liquid phase because liquid collagen is more costly than water and the surface contact angles are very close.

According to the results, the contact angles of collagen and deionized water were nearly the same, we continued with deionized water for contact angle measurements due to the low cost and ease of measurement for further experiments.

Rhodamine B was used for the confidence test. Figure 2.12 shows snapshots of the filling test of the chip having channel heights of 50/200 µm [Coskun et al., 2022].

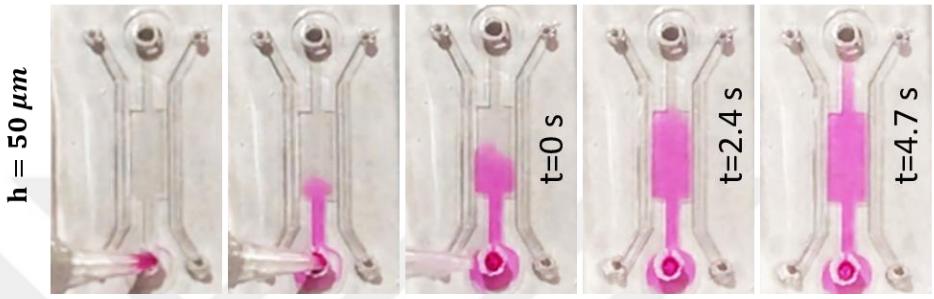

Figure 2.12: Snapshot images of loading with Rhodamine B solution obtained for the microfluidic chip with 50/200 µm channel heights [Coskun et al., 2022].

The confinement tests of the chips using wax as a mold are given in Figure 2.13. The chips in Figure 2.13 have a channel height of 150/400 µm and the design in Figure 2.13b has 4 grooves with a diameter of 300 µm.

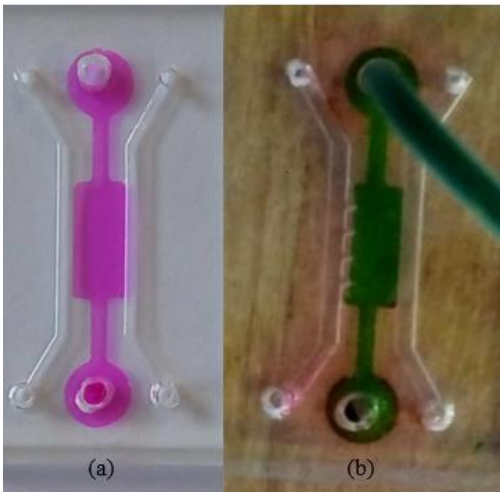

Figure 2.13: Images of a) Loading with Rhodamine B dye of the design with h=150/400 µm height, (b) Loading with green food dye-stained water of the design with h=150/400 µm height and 300 µm diameter grooves

As a result, filling tests of microfluidic chips with different channel heights were successful. However, the central channel of the grooved design in Figure 2.13b is not completely filled. Microscope images in Figure 2.14 show that the water does not pass around the grooves, and it causes a confinement problem. After the confinement test of

this design, images of the grooves were obtained using a light microscope. In Figure 2.14, the images of the grooves are presented before and after filling. As seen in Figure 2.14, water could not penetrate between the grooves. Therefore, in the following experiments, finer tips were used for CNC, the number of grooves was reduced, and their diameters were enlarged. The water confinement test of the microfluidic chip with 600 µm diameter grooves is presented in Figure 2.15. The problem of water not penetrating between the grooves has been solved.

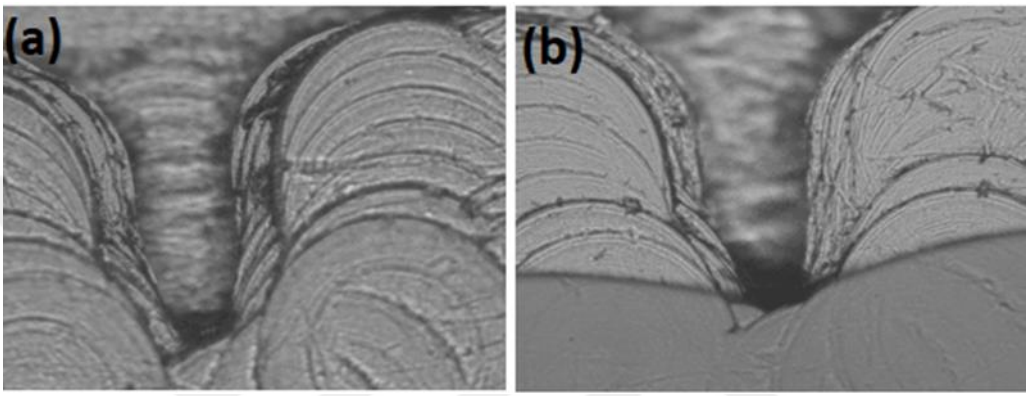

Figure 2.14: Images of (a) before loading (b) after loading with green food dye-stained water of grooves with h=150/400 µm height and 300 µm diameter width.

Figure 2.15: Image of h=150/400 µm channel heights of three grooves having 600 µm diameter loading with Rhodamine B dye-stained water.

2.4.3 Diffusion Tests

For the design with h=50 µm center channel height, the diffusion of water was observed using dyed water at different speeds at a constant flow. After adding collagen

to the central channel, using a syringe pump from the side channel at continuous rates of 0, V, 10V, and 50V, dyed water was given with V=185 µm/s. In Figure 2.16, images from the side channel (a) speed=0 (b) speed=V (c) speed=10V (d) speed=50V after the start of dyed water is given 2 minutes later are presented [Coskun et al., 2022].

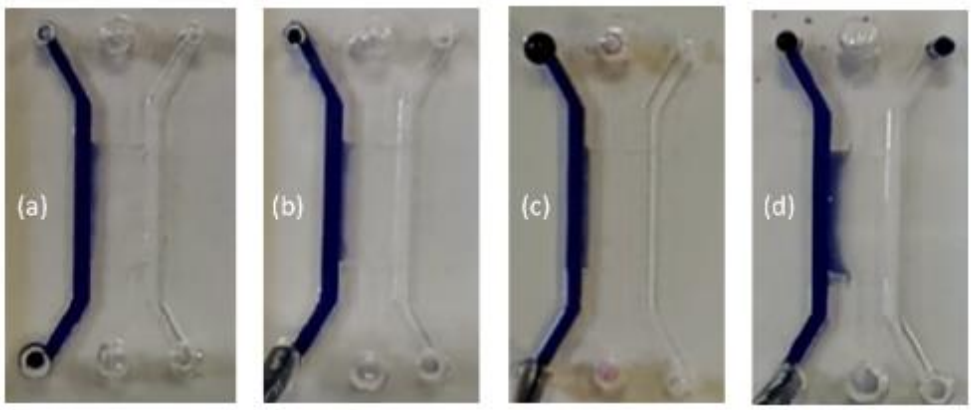

Figure 2.16: Diffusion of dyed water through the hydrogel under constant flow rates. The mean velocity of the dyed water is (a) 0, (b) 1V, (c) 10V, and (d) 50V, where V = 185 µm/s [Coskun et al., 2022].

According to diffusion experiments, increasing the flow rate increases the diffusion of the dyed water through the hydrogel. Also, it proves the ability to control chemicals with different flow rates by using side channels.

2.4.4 3D Cell culturing

2.4.4.1 Human aortic primary vascular culturing of flat muscle cells in a microfluidic chip environment

Human aortic primary vascular smooth muscle cells (HAPVSM) were grown in a 2D cell culture medium. Cells were seeded in cell culture dishes (T75 flask) with a surface area of 75 cm^2 at $7x10^5$ cells / T75. A vascular smooth muscle basal growth medium (Vascular Basal Medium, ATCC) containing 2% fetal bovine serum (FBS) was used for smooth muscle cells. After the cells were grown in 2D culture, they were seeded into microfluidic chips, as explained in the materials and methods section. The smooth muscle cells placed in the collagen channel of the microfluidic chip were shown to be healthy in the imaging performed two days later, as shown in Figure 2.17. Structures marked in red are actin filaments.

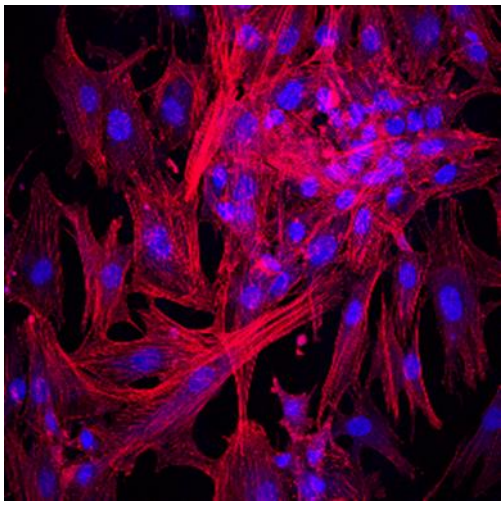

Figure 2.17: Confocal microscope image (20X) of cells fixed two days after.

2.4.4.2 Investigation of the response of HUVEC cells on the hydrogel in the microfluidic chips to TNF-α

This experiment investigated HUVEC cells placed on collagen hydrogel formed in the central channel of a microfluidic chip, and their response to a chemical stimulus from the opposite channel was followed by imaging. HUVEC cells were placed in the microfluidic chips containing collagen as described in the previous section. TNF-α (PeproTech) was added to the opposite channel containing HUVECs at a concentration of 1 µg/ml in endothelial cell growth medium containing 5% fetal bovine serum (FBS) Penicillin/streptomycin. After 44 hours in the incubator, HUVEC cells were labeled with calcein. Calcein is a living cell indicator. It was added to the cell channel in acetoxymethyl ester (Calcein-AM, Invitrogen). This form crosses the cell membranes and transforms into a free and calcium-interacting form with the effect of esterases inside the cell. After adding calcein to the HUVEC cell channel, the microfluidic chips were incubated for 30 minutes that which was not internalized and removed from the channel with endothelial cell growth medium. Cells were examined under a Leica confocal microscope (Leica DMi8 SP8) in the live-cell imaging mode (viewing field at 5% CO_2,and 37°C).

TNF-α has been shown to have an apoptotic effect on endothelial cells [Miyazaki et al., 2017]. The microfluidic chip design expected that TNF-α administered to the opposite channel would pass through the collagen and affect HUVECs. This protein has 17.5 kDa in size, and it passes through the pores of the collagen and acts on the cells. The effect of the TNF-α on the cells results with decreasing in the number of living cells. In the

experiments, it was shown that TNF-α administration for 44 hours reduced the viability of HUVEC cells (Figure 2.18).

This section reports two cell studies on microfluidic chip functionality with smooth muscle cells and HUVECs. These results show that a microfluidic chip design with three parallel channels allows the three-dimensional culture of different cells and helps to observe the effects of various chemicals on cells [Coskun et al., 2022].

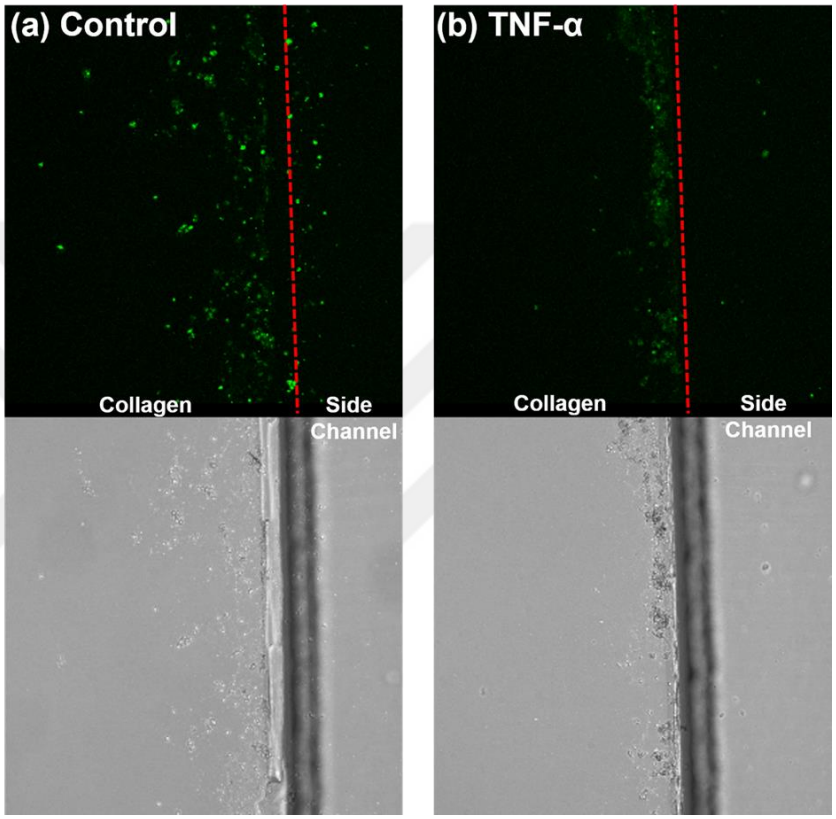

Figure 2.18: Images(10X magnification) of (a) Control chip. (b)Chip with TNF-α added [Coskun et al., 2022].

2.5 Discussion

In this chapter, we successfully fabricated PDMS-based microfluidic chips for different cell applications, such as human aortic primary vascular culturing of flat muscle cells. We investigated the response of HUVEC cells to the hydrogel in the microfluidic chips to TNF-α. Our 3-channel structure design is easy to fabricate using tapes with different thicknesses. We tested the channel heights by using a profilometer. The profilometer results show that we precisely fabricated the molds with a digital craft cutter and CNC. We continued to the fabrication of molds for design with grooves. PDMS is easy to produce, and the oxygen plasma treatment surface can be modified to increase hydrophilicity and bonding. The confinement tests were successful for both water and

collagen. After loading collagen successfully, the cells were given from the side channel. Due to the different heights between the side and central channels, the cells diffused through the collagen. We tested the diffusion of dye water with different fluid velocities, and we showed that increasing velocity increases the diffusion rate; it acts like laminar flow as expected. For another application, the side channel was used for investigating the effect of TNF response. The microscope images of the cells show that the microfluidic platform we fabricated can be used for the gradient of various chemicals. In addition, by using these microfluidic chips, we can mimic the cell environment. For future studies, we will change the material to PMMA due to hydrophilicity and repeated usage. Chapter 3 focused on PMMA-based microfluidic chip fabrication for cell experiments.

Chapter 3

PMMA MICROFLUIDIC CHIPS FOR 3D CELL CULTURING

3.1 Microfluidic Chip Design for 3D Cell Culturing

This section aims to fabricate the previously mentioned 3-channel design using PMMA material. It aimed to create a suitable micro-environment for cell studies using the solvent bonding technique, which is extremely easy and requires a small amount of material. There is a study in which PMMA was bonded in 15 minutes with the help of paper clips using different percentages of IPA and ETOH. According to this study, PMMA heated with a 65°C oven was irreversibly bonded in 50% and above IPA and 60% ETOH solution [Bamshad et al., 2016]. In another study, they bonded PMMA using different solvents for 2 min,5 min, and 7 min at 50°C, 60°C, and 70°C temperatures using an oven. In this study, plasma treatment was added to the procedure to increase the bonding strength. Different percentages of DCM, IPA, and ACE mixtures were prepared, and the Hildebrandt parameter was used to decide the rates [Faghih and Sharp,2018]. As mentioned, the Hildebrandt parameter gives information about whether the solvent and the material will bond. The mixture with the desired Hildebrandt parameter can be obtained using different percentages of liquid mixtures. This study used different ratios of mixed IPA, ETOH, and ACE. Since there are studies that acetone increases bonding strength, ACE additions were made for IPA and ETOH.

In addition, we added plasma treatment to the procedure to investigate the effect. Paper clamps were used to apply the pressure. Each paper clamp applies an average force of 27N. Four paper clamps were used for 25 mm*75 mm PMMA, so 57.6 KPa was applied for each PMMA. Microscope slides were placed at the top and bottom to distribute the pressure equally on the surface. No PMMA microfluidic chip is fabricated in the literature with solvent bonding technique at two different heights. In addition, only a few studies on constructing PMMA microfluidic platforms are used in cell studies fabricated by solvent bonding techniques. This is a challenge as the solvents used for PMMA microfluidic fabrication are harmful to cells. In this study, microfluidic chips with two different heights were fabricated for cell study with the solvent bonding technique, which is a remarkably cheap and easy method. Microfluidic chip design was processed using CNC, which is a precise method and provides high resolution. As a final step, the

retention groove was added to the design, improving solvent entrapment, and increasing bonding coverage [Bamshad et al., 2016]. Figure 3.1 shows the AutoCAD design of the microfluidic chip we used for the cell studies.

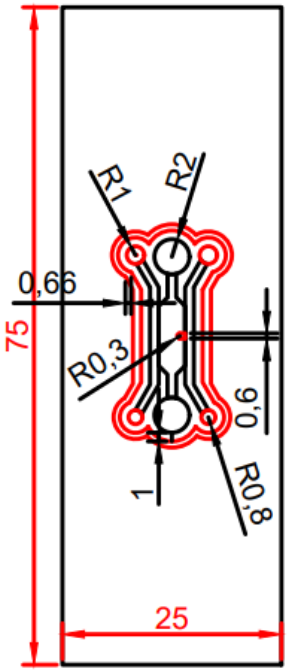

Figure 3.1 AutoCAD design of the microfluidic chip (mm dimensions).

3.2 Materials and Method

2 mm thick PMMA was obtained from Filiz Plastik. Parts of different sizes used in this work were cut with Almire Laser 590. The purities of solvents are 96%. Roland MDX-50 branded CNC machine was used to process PMMA. The ultrasonic bath used in the cleaning part is ISOLAB brand, and the power is 120 W. The brand of pipette tips used when preparing solvent in filling tests is Biosphere. Nikon Eclipse TE2000-U microscope was used for images taken at 20X, and Zeiss Axio Imager M1 branded microscope was used for 5X images. The cells within the microfluidic chip were imaged using an inverted fluorescence microscope (Zeiss Axio Observer Z1) with a 10X objective. Shimadzu model AGS-X was used in bonding strength experiments.

3.3 Microfluidic Chip Fabrication

3.3.1 Preparation of mold

The design with two different height channels and grooves is drawn in AutoCAD. PMMA is cut in 25x75 mm dimensions with a laser. The two-layer design mentioned

using CNC is machined on the PMMA. Since residue remained in the channels due to CNC, PMMA waited in the ultrasonic bath for 10 minutes after processing. After the ultrasonic bath, PMMA is washed first with IPA and then DI. The final step is drying the chips in a 50°C oven. Figure 3.2 shows the CNC machined PMMA after and before cleaning.

Figure 3.2: CNC machined PMMA having 150/400 µm channel heights, 1 groove 600 µm diameter, 70 µm retention length, and 50 µm height d a) before cleaning b) after cleaning.

3.3.2 Solvent Bonding Technique

The solution obtained by mixing IPA, ACE, and ETOH liquids at different rates is prepared in a fume hood. Since these liquids are highly volatile, they were not stored. Mixtures were prepared before bonding experiments. 200 µl solvent is used for the 25×75 mm PMMA. 150 watts of oxygen plasma is applied to both surfaces of the pre-cleaned PMMA for 60 seconds. Within 5 minutes after the treatment, the prepared solvent mixture is applied with a pipette to only one side. After pouring the solvent, the other PMMA part is covered in this plain. The next step is placing two microscope slides for the bottom and upper part of the PMMA and fastening it with four paper clips.

The setup shown in Figure 3.3a is kept in the oven at 65°C for 10 minutes, then left at room temperature for another 5 minutes with the paper clips attached. Then, the paper clips are removed, and the microfluidic chip is left in the oven at 50°C for 20 minutes to

evaporate the remaining solvent in the channels. Figures 3.3b and 3.3c shows images before and after the oven process. There is a significant difference between the two situations. After heating, no solvent in the structure causes clogging problems. Since this microfluidic chip will be used for cell studies, no solvent residue in the channels is critical. If solvent remains, the cells inside the chip will die over time. Therefore, there is a cleaning step after microfluidic chip fabrication. The chips are kept in DI for 10 minutes in an ultrasonic bath. After soaking in DI water overnight, they are kept in an ultrasonic bath for five more minutes. Finally, the chips are left in the oven at 50°C until dry.

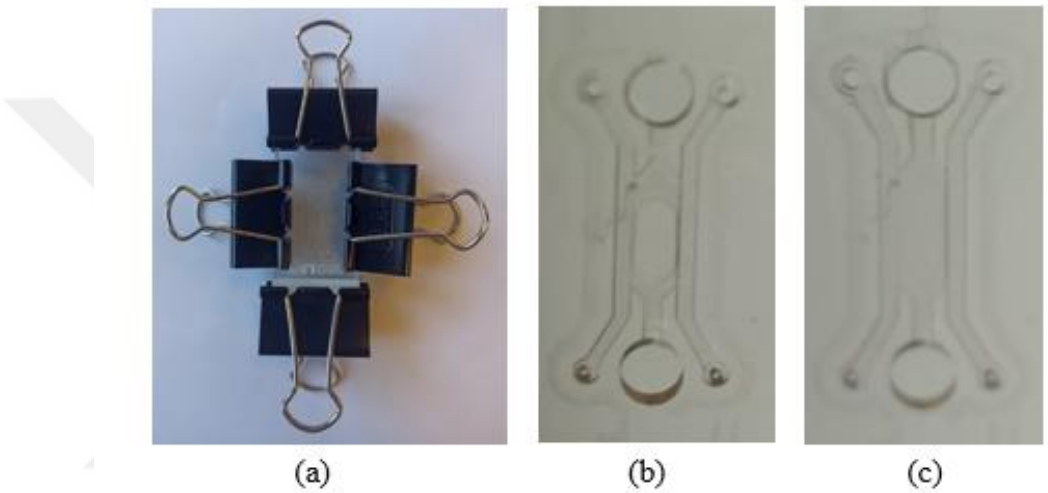

Figure 3.3: Setup of the solvent before bonding (a), image of microfluidic chip: before heating (b), after heating(c)

3.3.3 3D Cell Culturing

The materials and methods for 3D cell culturing are the same as in section 2.3.3

3.4 Results

3.4.1 Profilometer Measurements

The height profiles of the channels were measured with a Dektak profilometer over the CNC machined PMMA. The surfaces were scanned with a 12.5 µm stylus radius and 3 mg Stylus force for a length of 10000 µm and a duration of 70 s. Profilometer results prove that the middle (h=150µm), side channel height (H=400 µm), and groove height around 250 µm were obtained successfully. Profilometer results of the PMMA are given in Figures 3.4 and 3.5. Figure 3.5 shows that the retention groove has a 50 µm height.

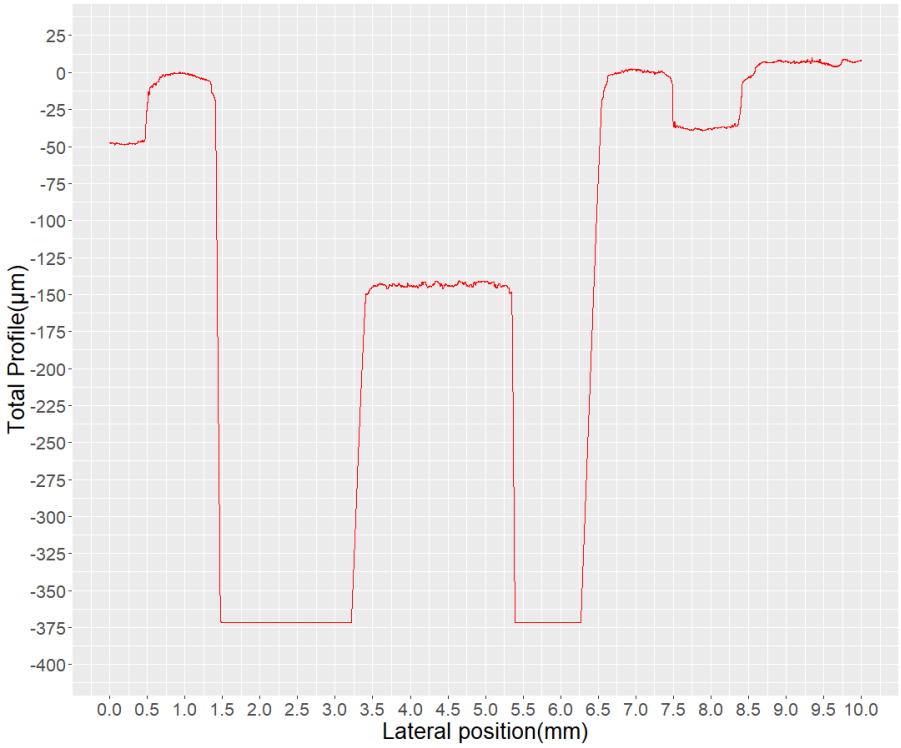

Figure 3.4 Profilometer measurement of PMMA having 50 µm groove retention and 150/400 µm channel height.

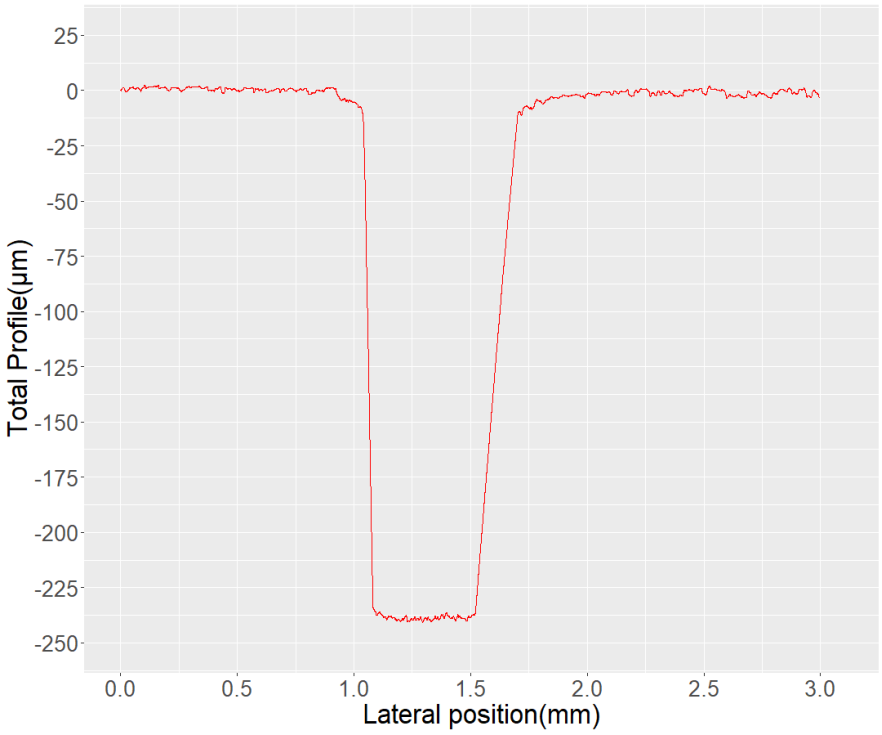

Figure 3.5: Profilometer measurement of PMMA in the middle channel direction having 50 µm groove retention and 150/400 µm channel height and 1 groove 600 µm diameter.

3.4.2 Bonding Coverage

In this section, PMMA was bonded with different solvents at different temperatures using the solvent bonding technique. Hildebrandt parameters were investigated to find the suitable solvent for PMMA-PMMA bonding. The solubility parameter of PMMA is 20.1 $J^{1/2}cm^{3/2}$. Therefore, the solubility parameter of the solvent for PMMA bonding should be close and close enough to this value. The Hildebrandt parameter of acetone is very close to PMMA, and a clogging problem arises in channel structures. The aim is to find solvents with good bonding coverage, bonding strength, and successful fillings. When calculating the Hildebrandt parameter of a mixture, the ratio is made according to the volumes. According to this ratio calculation, solubility parameters of mixtures in different percentages can be calculated. Hildebrandt parameters of ethanol and acetone mixtures prepared in different percentages and bonding coverage percentages concerning these mixtures are given in Table 3.1.

Table 3.1: Solubility parameters and bonding coverage percentages of different percentages of ETOH and ACE.

ETOH (volume %)	ACE (volume %)	Solubility Parameter ($J^{1/2}cm^{3/2}$)	Bonding Coverage (after plasma)	Bonding Coverage (no plasma)
0	100	20.4	98%	77%
10	90	20.96	93%	82%
20	80	21.52	81%	45%
30	70	22.08	80%	91%
40	60	22.64	95%	89%
50	50	23.2	98%	83%
60	40	23.76	79%	91%
70	30	24.32	95%	85%
80	20	24.88	97%	96%
90	10	25.44	91%	90%
100	0	26	51%	39%

PMMA pieces cut in 25x25 mm dimensions were bonded to using the solvents given in Table 3.1 by keeping them in an oven at 65°C for 10 minutes and room temperature for 5 minutes. Images of these PMMA parts are given in Figure 3.6. In Figure 3.6, the right sections were bonded without the plasma treatment. This section aims to find the effect of plasma treatment on bonding coverage.

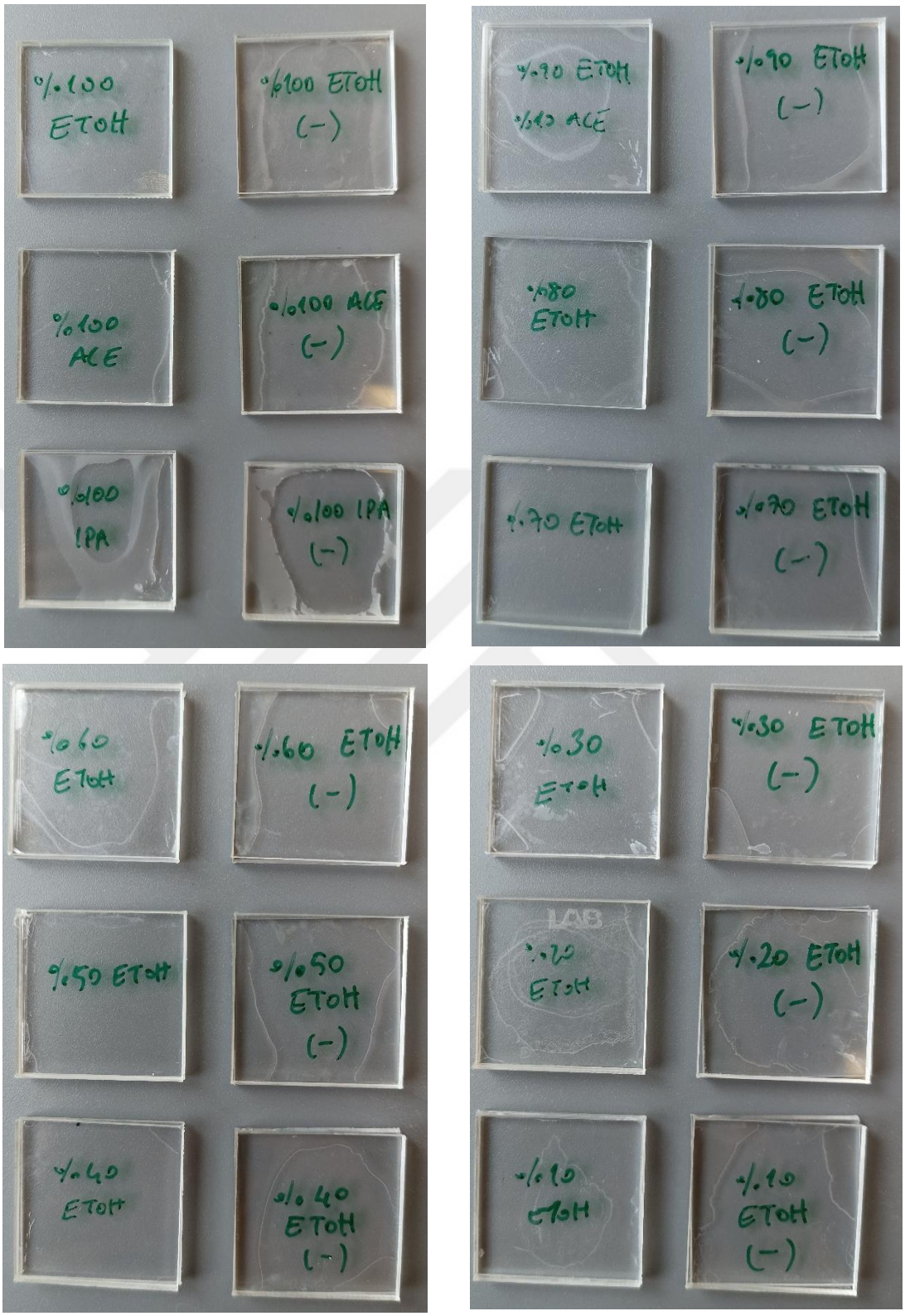

Figure 3.6: Bonding coverage image of PMMAs with different concentrations for ethanol and isopropyl alcohol mixing with acetone. The right section was bonded without plasma treatment.

One of the results is that bonding coverage is better for PMMA bonded with plasma treatment. For ethanol and acetone mixtures, better bonding coverage is obtained as the percentage of acetone increases. However, there is no significant difference between ethanol and acetone mixtures; for example, comparing 90% ETOH +10% ACE (91%) and 90% ACE+10% ETOH (97%) having plasma treatment, appears that there is only a 7% difference concerning bonding coverage. This is reasonably expected because acetone alone can bond PMMA very sufficiently. However, the best bonding coverage between mixtures of ethanol and acetone is 70% ETOH+20% ACE with plasma treatment.

Hildebrandt parameters of isopropyl alcohol and acetone mixtures prepared in different percentages and bonding coverage percentages concerning these mixtures are given in Table 3.2. Images of these PMMA parts are given in Figure 3.7, and the right sections were bonded without the plasma treatment. According to bonding coverage results, adding plasma treatment to the methods increase the bonding area. 90% IPA+10% ACE mixture has better bonding coverage than the mixture with no plasma treatment. Also, if the amount of acetone increases, bonding coverage has a better value when comparing 100% IPA and 40% IPA+60% ACE mixture.

Table 3.2: Solubility parameters and bonding coverage percentages of different percentages of IPA and ACE.

IPA (volume%)	ACE (volume%)	Solubility Parameter ($J^{1/2}cm^{3/2}$)	Bonding Coverage	Bonding Coverage (no plasma)
40	60	21.6	94%	96%
50	50	21.9	91%	93%
60	40	22.2	95%	95%
70	30	22.5	95%	90%
80	20	22.8	71%	78%
90	10	23.1	95%	82%
100	0	23.4	65%	70%

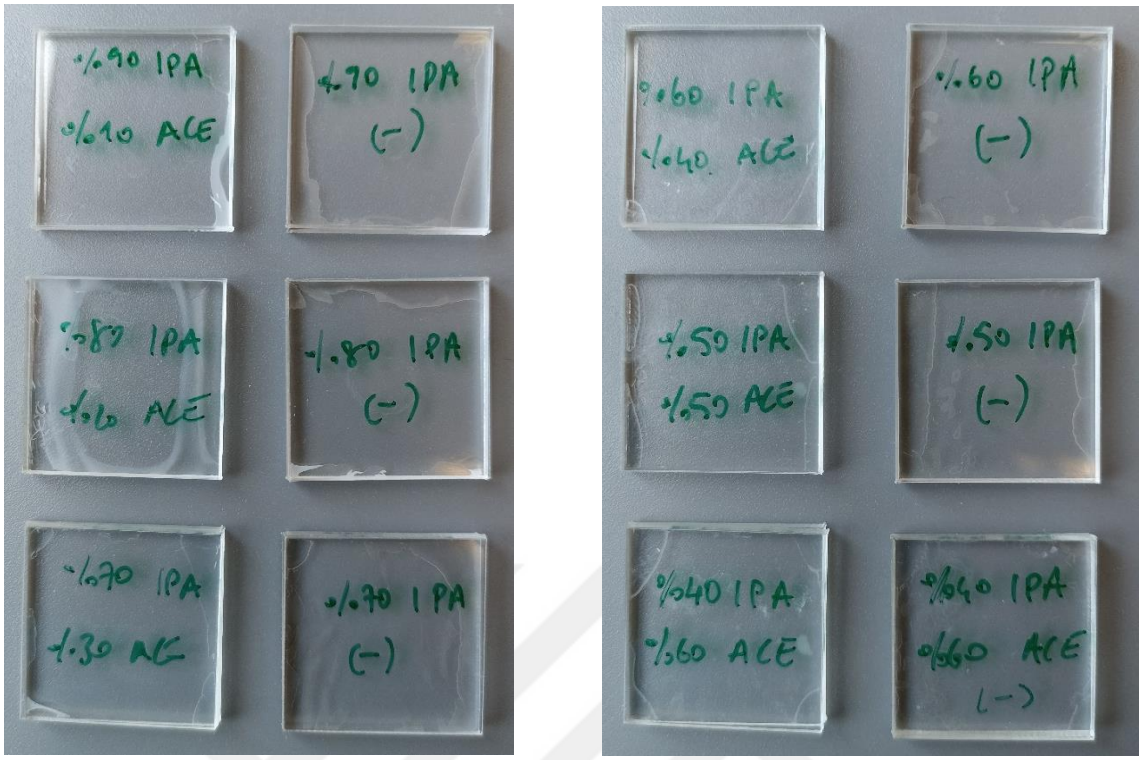

Figure 3.7: Bonding coverage image of PMMAs with different concentrations of isopropyl alcohol and acetone. The right part was bonded without plasma treatment.

One of the effects of solvent bonding is the condition of the surface. When a solvent is used for bonding, the material's surface is expected to have no damage. In order to examine this damage, microscope images of the bonded PMMA part were analyzed. Figure 3.8 shows 8 total bonding scenarios having different mixtures with and without plasma treatment.

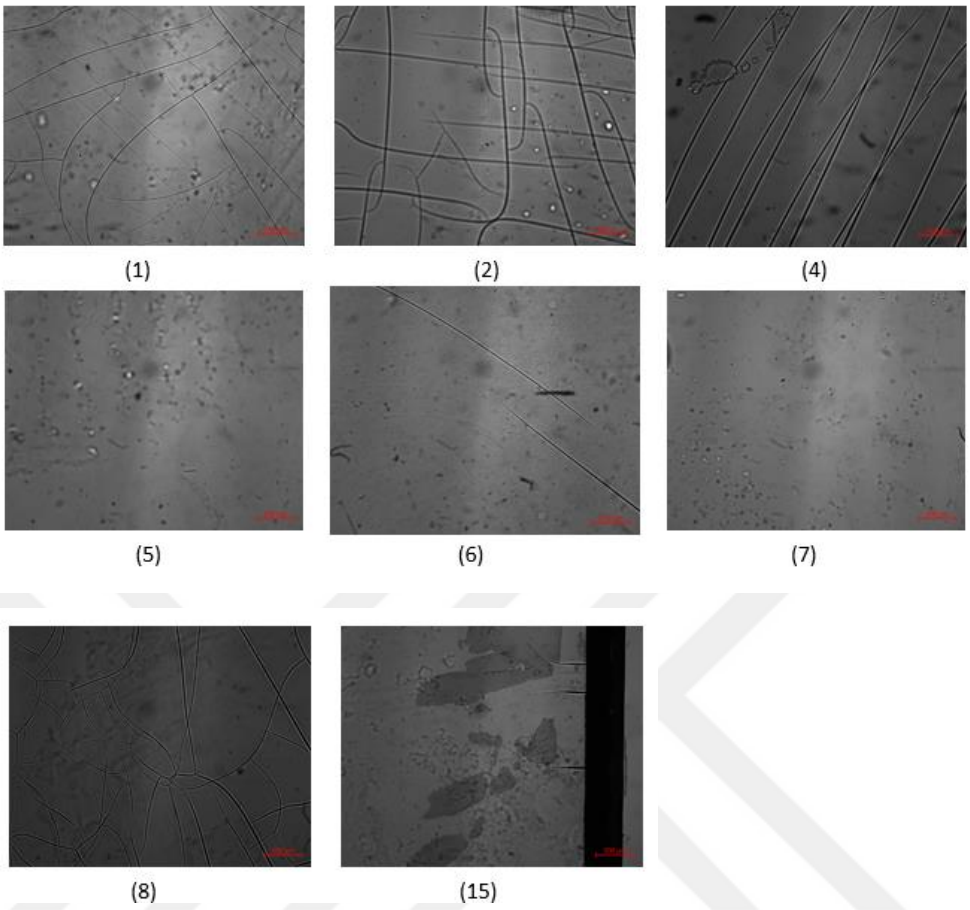

Figure 3.8 Microscope images (5X magnification) of different bonding scenarios. The number of samples refers to Table 3.3.

By examining the microscope images of 100% IPA, 100% ACE, and 100% ETOH, the most damaged bonded PMMA is 100% ACE. The best solvent is 100% ETOH according to minimizing surface damage. Comparing samples 2 and 8 reveals the effect of acetone on the surface. By looking at microscope images of these samples, it was proved that increasing the volume of acetone causes more damage to the bonding area. Also, plasma treatment minimizes the damage to the surface. Samples 2 and 5 have the same parameters except for the plasma treatment. Plasma treatment is a solution for minimizing the damage.

3.4.3 Bonding Strength

Mixtures to be tested for bonding strength tests were selected according to Hildebrandt parameters. In addition, the effects of both plasma treatment and temperature were examined regarding bonding strength. Table 3.3 shows the bonding cases with different temperatures, plasma treatments, and solvent types.

Table 3.3: Samples for using bonding strength experiments.

Sample No	Solvent Type	Hildebrand Solubility Parameter ($J^{1/2}cm^{3/2}$)	Temperature (°C)	Plasma Treatment
1	100% IPA	23,4	65	no
2	80% IPA+20% ACE	22,8	65	no
3	40% IPA+60% ACE	21,9	65	no
4	40% ETOH+60% ACE	22,64	65	no
5	80% IPA+20% ACE	22,8	65	yes
6	40% ETOH+60% ACE	22,64	65	yes
7	80% ETOH+20% ACE	24,88	65	no
8	100% ACE	20,4	65	no
9	40% IPA+60% ACE	21,9	room	no
10	40% ETOH+60% ACE	22,64	room	no
11	80% IPA+20% ACE	22,8	room	yes
12	40% ETOH+60% ACE	22,64	room	no
13	80% ETOH+20% ACE	24,88	room	no
14	100% ACE	20,4	room	no
15	100% ETOH	26	65	no

Bonding strength experiments were done according to ASTM D3163(Determining Strength of Adhesively Bonded Rigid Plastic Lap-Shear Joints in Shear) standard. PMMA parts with 25×100 mm dimensions were bonded with 25×25 mm areas. Pictures of PMMAs before and after bonding strength measurement are given in Figure 3.9. Also, the percentages of these overlapped areas show the bonding coverage. As seen in Figure 3.9, irreversible bonding occurred during all bonding strength experiments. In the literature, some studies state an irreversible bonding situation [Bamshad et al., 2016 and Trinh et al., 2021]. Microscope images were taken from the bonding area to understand the reason beyond this case. Table 3.4 shows applying force needed to break the bonding, lap shear strength, and elongation failures with comments.

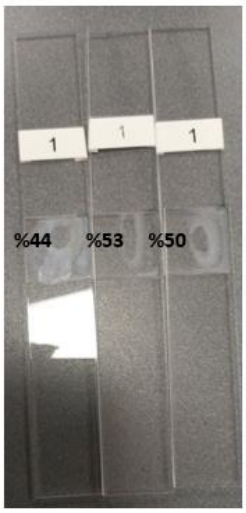
1
1
1
%44
%53
%50


2
2
2
%55
%57
%41


3
3
3
%52
%61
%77


4
4
4
%74
%57
%55

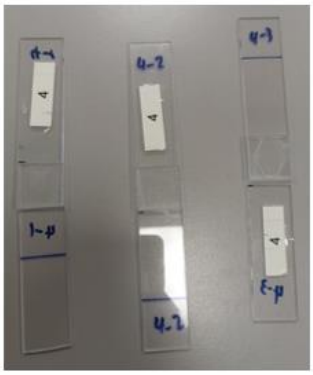

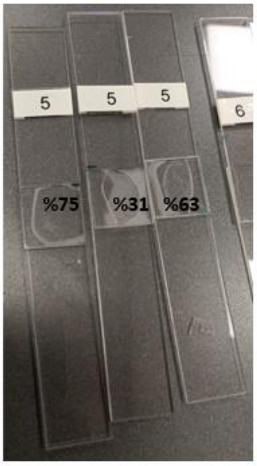
5
5
5
%75
%31
%63


6
6
6
%93
%66
%92

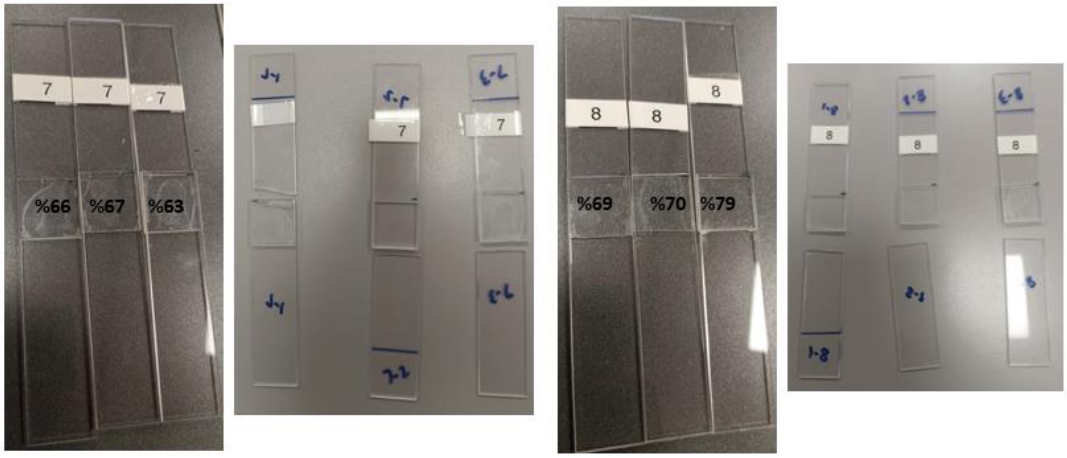

Figure 3.9: Pictures of bonded PMMA (25×25mm) before and after bonding strength experiments with a heated oven.

Table 3.4: Bonding strength results for PMMA with heat bonded.

Sample no	Force (N)	Lap-Shear Strength (MPa)	Elongation at failure (mm)	Comments
1-1	211.9	0.339	0.88	Adhesive failure
1-2	285.2	0.456	1.02	PMMA failure
1-3	Adhesive failure during clamping			
2-1	686.6	1.099	1.66	PMMA failure
2-2	963.4	1.541	2.17	PMMA failure
2-3	1081	1.730	2.54	PMMA failure
3-1	1258	2.012	2.48	PMMA failure
3-2	1151	1.842	2.72	PMMA failure
3-3	950.3	1.521	1.97	PMMA failure
4-1	937.6	1.500	1.99	PMMA failure
4-2	1359	2.175	2.63	PMMA failure
4-3	743.5	1.190	1.70	PMMA failure
5-1	678.5	1.086	1.52	PMMA failure
5-2	561.2	0.898	1.50	PMMA failure
5-3	709.8	1.136	1.88	PMMA failure
6-1	799.6	1.279	2.22	PMMA failure
6-2	717.6	1.148	1.80	PMMA failure
6-3	936.8	1.499	2.24	PMMA failure
7-1	1301	2.082	2.53	PMMA failure
7-2	1375	2.200	2.65	PMMA failure

7-3	651.7	1.043	1.52	PMMA failure
8-1	993.0	1.589	2.00	PMMA failure
8-2	1128	1.804	2.25	PMMA failure
8-3	1194	1.910	2.38	PMMA failure

Since these results are not related to the bonding area due to fraction points, they cannot be compared concerning parameters such as solvent type and plasma treatment. There is only one outcome: all the scenarios were bonded so well that they cannot be separable.

In order to get the relation between bonding strength and temperature, samples from Table 3.4 were bonded at room temperature instead of using the oven. Only scenarios worked with room temperature, as seen in Figure 3.11. All of the bonded samples have at least 60% of ACE. This result shows that increasing ACE volumes in the mixture give rise to better bonding strength. Also, comparing bonding strength in terms of plasma treatment has no effect since there is no bonded scenario having plasma treatment. Figure 3.10 shows the bonding coverage for each sample. These values were found for comparing bonding coverage and bonding strength, but there is no link between them. For example, sample 11 has higher bonding coverage than other cases, but the result shows no bonded area.

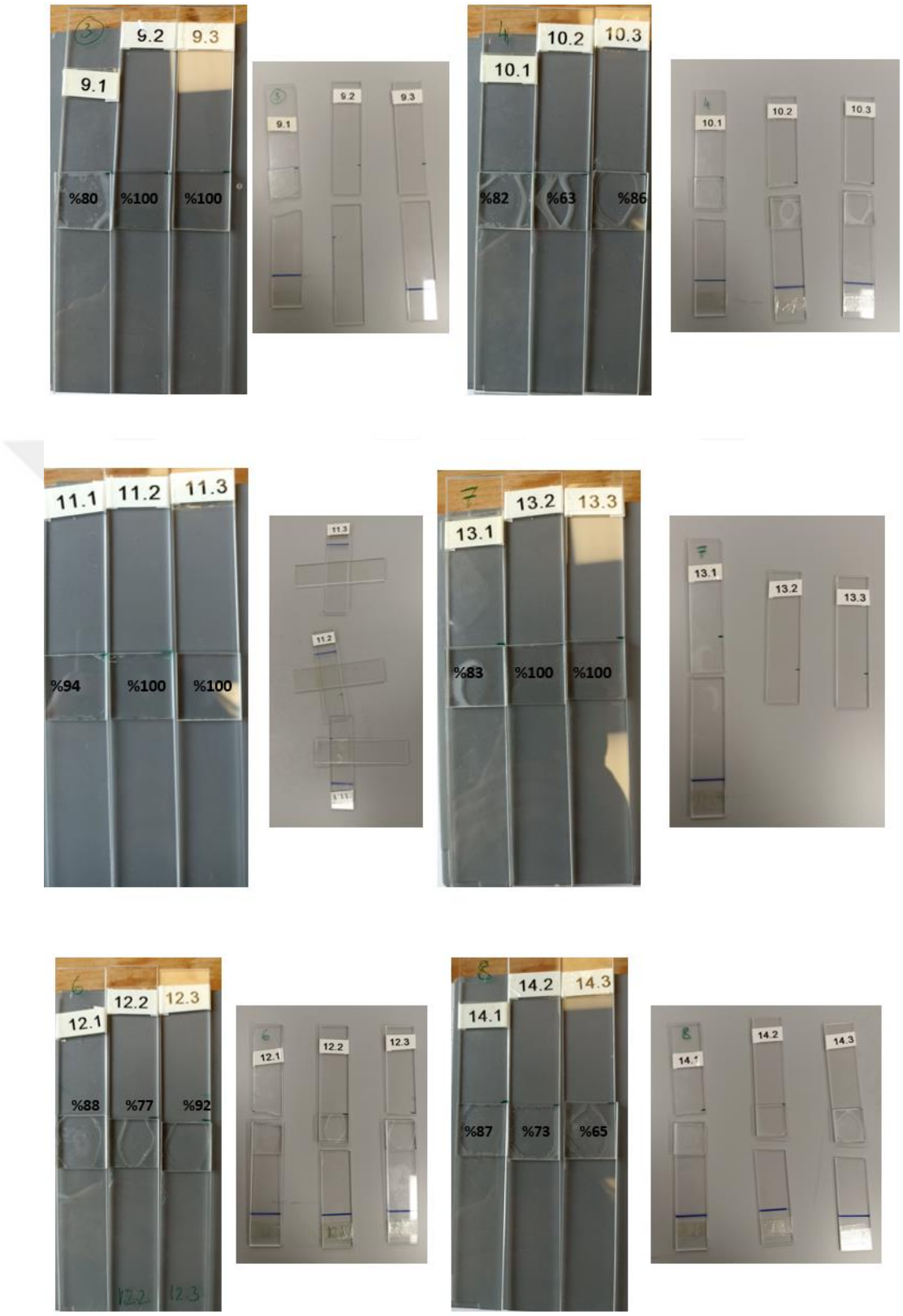

Figure 3.10: Pictures of bonded PMMA (25×25mm) before and after bonding strength experiments with room temperature.

Tablo 3.5: Bonding strength results for PMMA with room temperature.

Sample No	Force(N)	Lap-Shear Strength (MPa)	Elongation at failure (mm)	Comments
9-1	782.7	1.252	1.70	
9-2	Adhesive failure before clamping – No adhesion			
9-3	Adhesive failure before clamping – No adhesion			
10-1	603.3	0.965	1.50	PMMA failure
10-2	680.0	1.088	1.82	PMMA failure
10-3	604.9	0.968	1.55	PMMA failure
11-1	Adhesive failure before clamping – No adhesion			
11-2	Adhesive failure before clamping – No adhesion			
11-3	Adhesive failure before clamping – No adhesion			
12-1	656.8	1.051	1.62	PMMA failure
12-2	739.7	1.184	1.80	PMMA failure
12-3	848.8	1.358	2.24	PMMA failure
13-1	82.48	0.132	0.75	No adhesion
13-2	Adhesive failure before clamping – No adhesion			
13-3	Adhesive failure before clamping – No adhesion			
14-1	971.8	1.555	2.22	PMMA failure
14-2	645.2	1.032	1.70	PMMA failure
14-3	727.1	1.163	1.91	PMMA failure

Microscope images were taken after bonding strength experiments to find a reason beyond the irreversible bonding. Comparing these images with the before bonding case shows more damage close to the paper clamps. Sample 1 differs before and after the experiment, especially concerning its edge. The difference between Samples 8 and 14 is the temperature, so the solvent remains for almost one day for room temperature bonding. Extra time with solvent causes more damage to the bonding area. Considering microscope images of samples 2 and 7, one can understand that adding ethanol to the mixture minimizes the damage. Also, as in samples 2 and 3, an increase in ACE causes cracks in the bonded area.

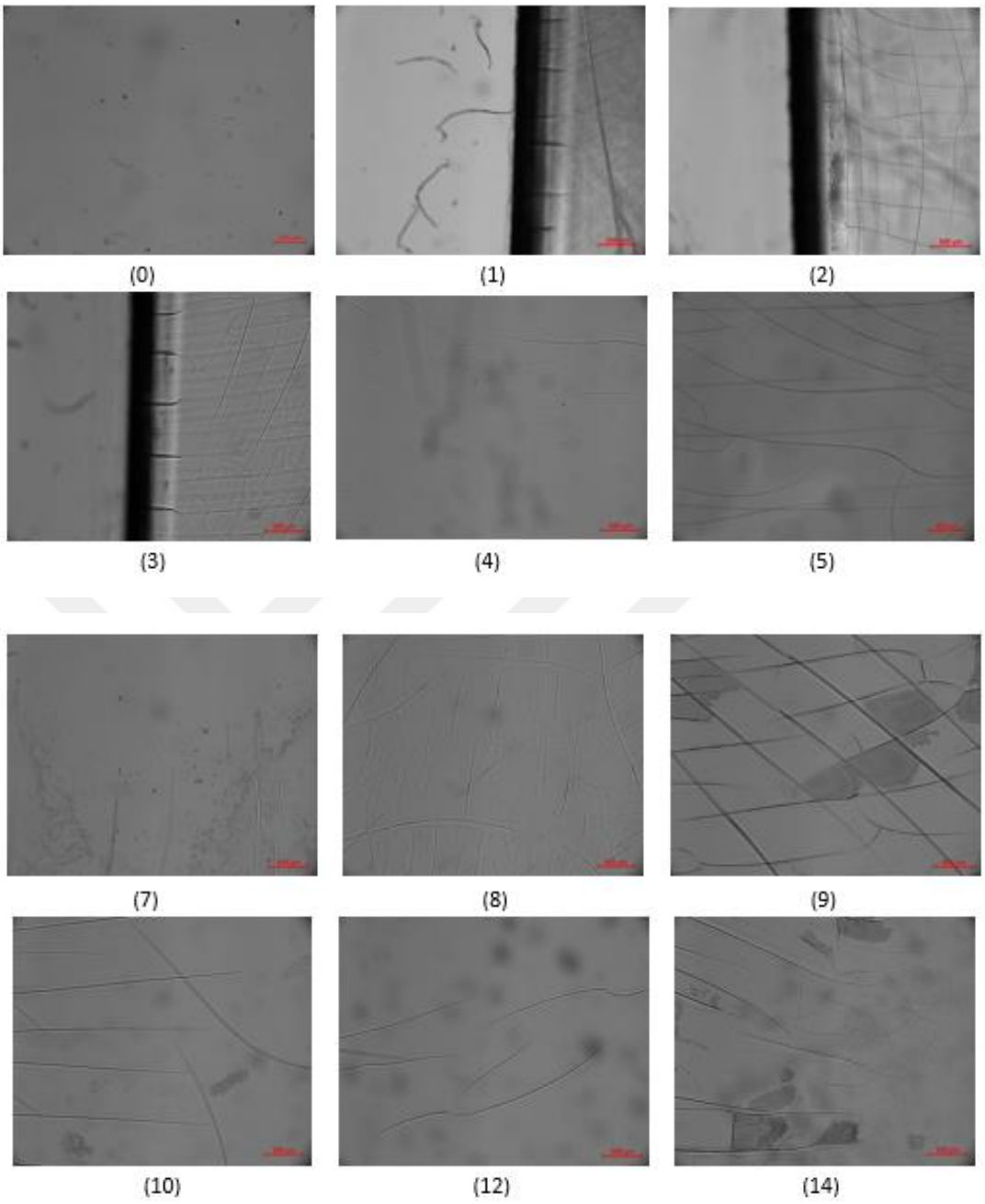

Figure 3.11: Microscope images (5X magnification) of different bonding scenarios after bonding strength experiments. The number of samples refers to Table 3.3.

3.4.4 Confinement Tests

3.4.4.1 Contact Angle Measurements

In order to know the wettability, the contact angles of PMMA were measured. Figure 3.12 shows the water droplets of the PMMA surface. The water contact angle was measured using these images with image-j. The values of contact angles are shown in Figure 3.13, and the average water contact angle for PMMA is 62.4°.

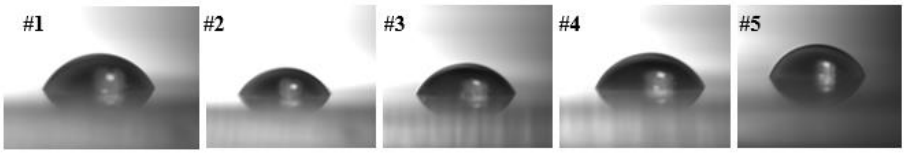

Figure 3.12: Images of 3 µl water drops dropped on ten different points of 2 mm thick PMMA.

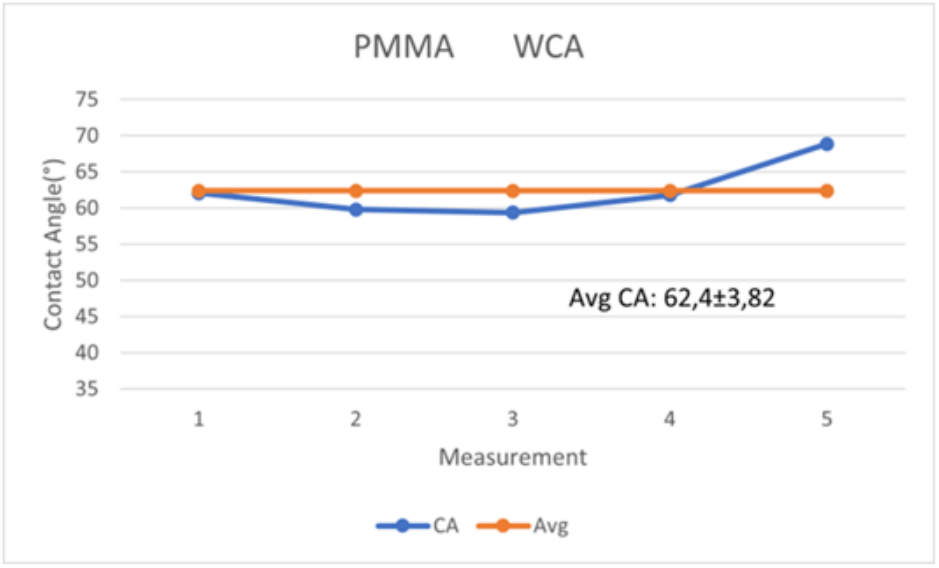

Figure 3.13: Water contact angles were measured from 5 different points of 2 mm thick PMMA. The average contact angle was measured as 62.4°.

The contact angle was measured with time to investigate the effect of the plasma treatment. Figure 3.14 shows the water contact angle with time after plasma treatment. The contact angle increases until the steady state after plasma treatment. According to these results, it takes about one week for the PMMA surface to stabilize. PMMA was bonded after plasma treatment immediately, so this hydrophilicity increases the coverage of the solvent.

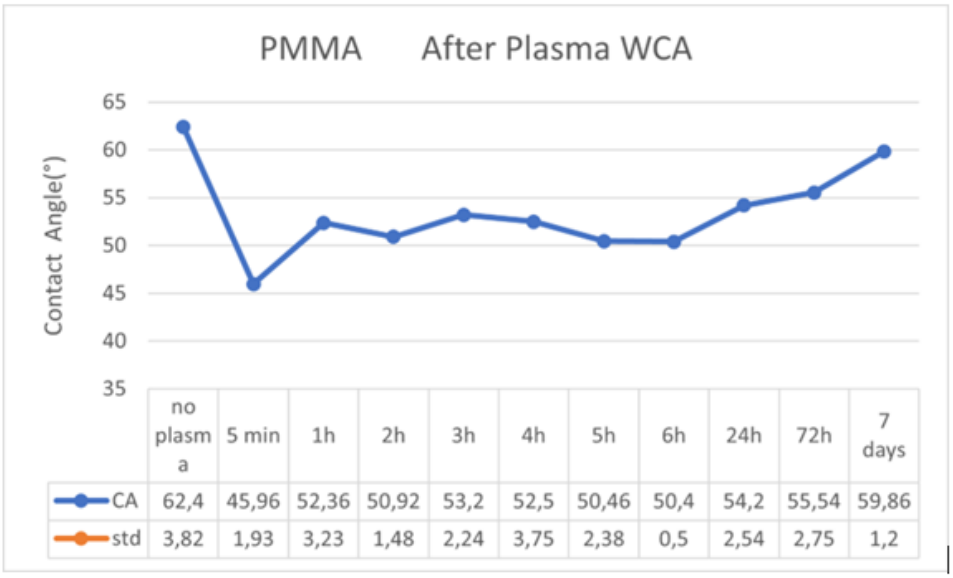

	no plasma	5 min	1h	2h	3h	4h	5h	6h	24h	72h	7 days
CA	62,4	45,96	52,36	50,92	53,2	52,5	50,46	50,4	54,2	55,54	59,86
std	3,82	1,93	3,23	1,48	2,24	3,75	2,38	0,5	2,54	2,75	1,2

Figure 3.14: Contact angles of PMMA after plasma treatment with time.

Also, it is essential that the effect of machining PMMA to contact angle. The water contact angle was measured after CNC machining to understand this relationship. After the surfacing process, the contact angle increases due to different surface locations affecting the droplet contact. The average water contact angle is 83.25° after CNC, as shown in Figure 3.15.

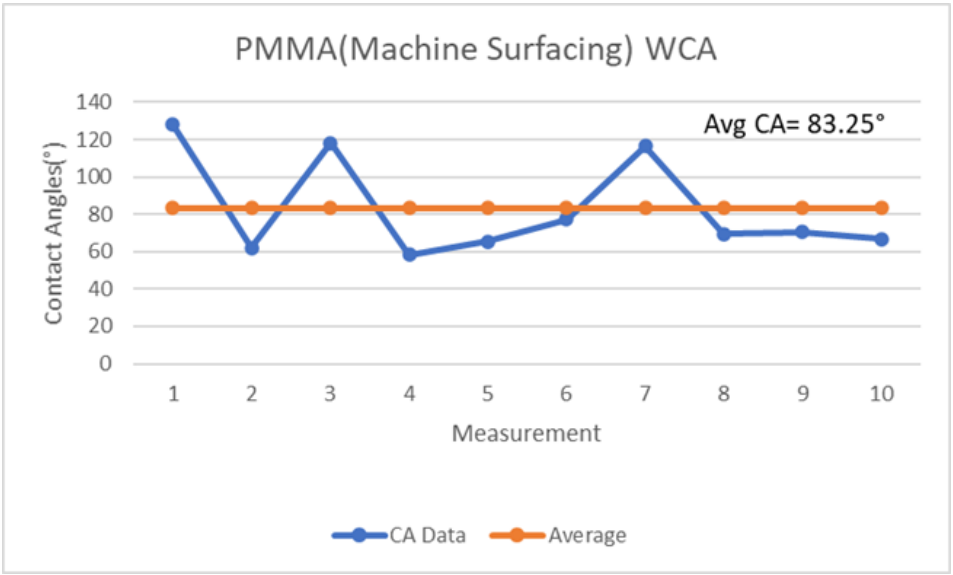

Figure 3.15: Water contact angle measurements of CNC machined PMMA surface.

In this study, the plasma power is 150W, and the duration is the 60s. Different powers (100W,150W,200W) and times (the 30s,60s, and 120s) were used to measure water

contact angles to investigate better plasma parameters. Table 3.6 shows the water contact angles of PMMA with different plasma power and time.

Table 3.6: Contact angles of PMMA with different plasma parameters such as plasma power and time.

Time (s) / Power (W)	30 s	60 s	120 s
100 W	53,03±1,15	46,03±0,85	44,26±2,26
150 W	47,03±1,46	46±0,14	44,66±2,48
200 W	47,8±0,26	47,3±0,95	46,6±0,41

According to Figure 3.16, increasing plasma power did not change the contact angle, especially for 60 s. However, comparing 100 W and 150 W plasma power for the 30s, the contact angle decreases when plasma power increases. Another result is that increasing plasma time decreases the contact angle for all plasma powers.

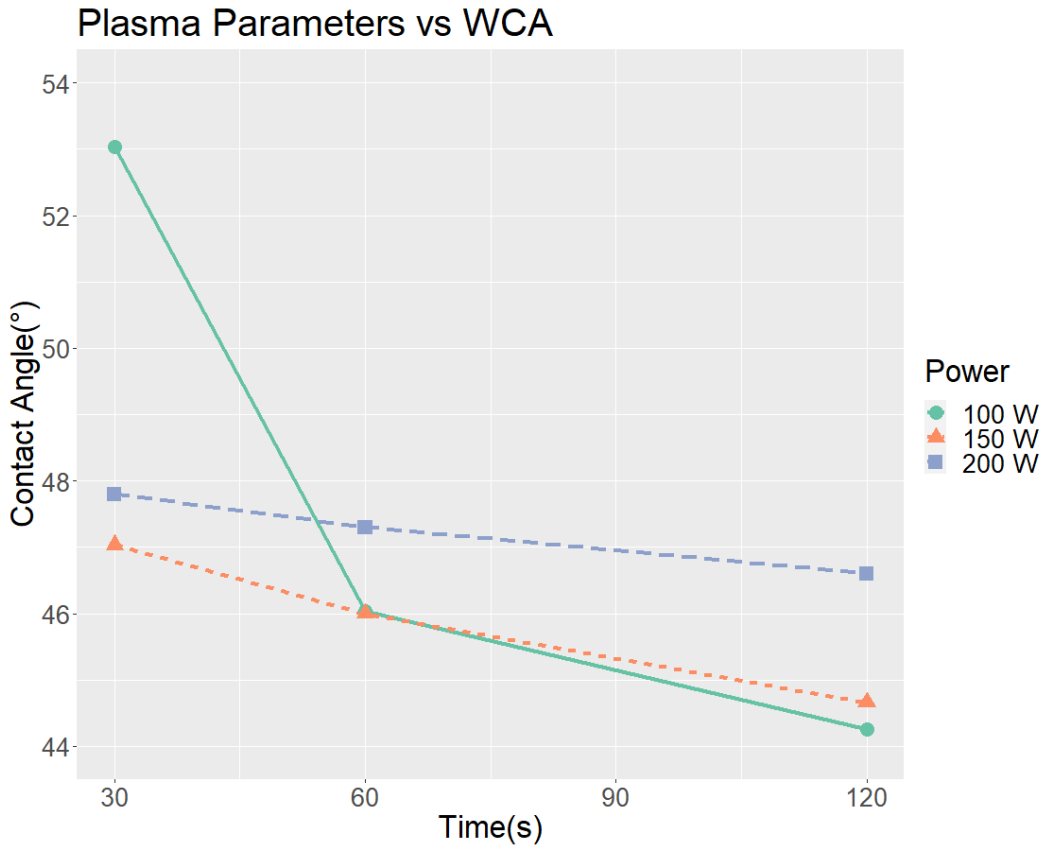

Figure 3.16: Contact angles of PMMA with different plasma powers and time

3.4.4.2 Confinement Tests

According to the results of bonding coverage, damage to the surface, and bonding strength, cases were selected for confinement tests. Understanding the acetone effect, 100% ACE and 40% ETOH +60% ACE were selected. 80% IPA +20% ACE mixture was bonded with and without plasma treatment to investigate the plasma effect. 80% ETOH+20% ACE mixture was selected to discover the effect of ETOH. In addition, the parameters effect of retention grooves was also investigated.

Microscope images of the cross-section of the microfluidic chip bonded with an 80% IPA+20% ACE mixture are given in Figure 3.17. There are two designs in one PMMA microfluidic due to finding the effect of the retention groove. The top of the drawing has a retention groove over the design. One can calculate the height of the side and middle channels from cross-section images. The height of the side channel is 392 µm, and the central channel is 142 µm for the chip with a retention groove. For the bottom design, the height of the side channel is 375 µm, and the main channel is 125 µm. Using an 80% IPA+20% ACE mixture did not damage the channels. In addition, adding retention grooves to the design prevented the solvent-induced filling problem in the channels by ensuring that the solvent remained in the frame, not in the channels.

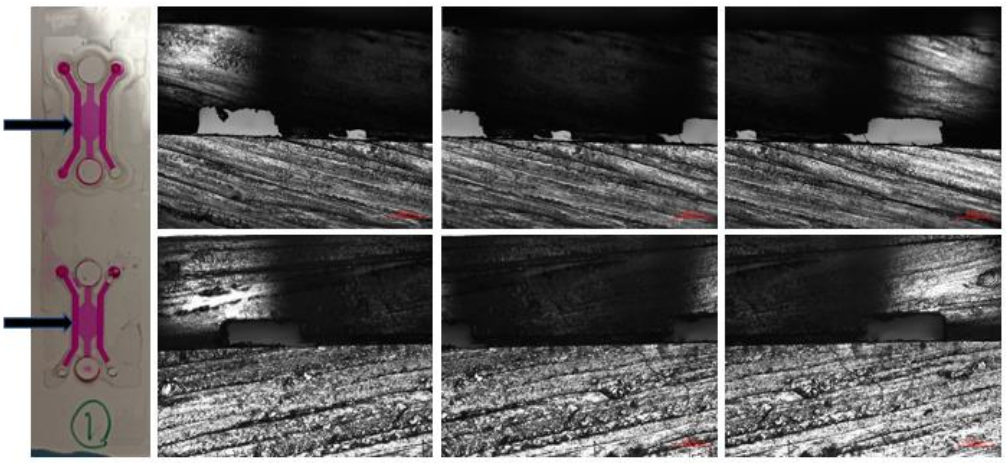

Figure 3.17: Cross-section images (5X magnification) of bonded PMMA (150/400 µm) with 80% IPA+20% ACE with plasma treatment.

Microscope images of the cross-section of the microfluidic chip bonded with a 40% ETOH+60% ACE mixture are given in Figure 3.18. For the bottom design, the height of the side channel is 326 µm, and the main channel is 110 µm. 60% ACE+40% ETOH mixture damaged the channels, especially with the assistance of the retention groove.

Since ACE is a more aggressive liquid than ETOH, the high percentage of acetone in the mixture used in bonding created a clogging problem in the channels.

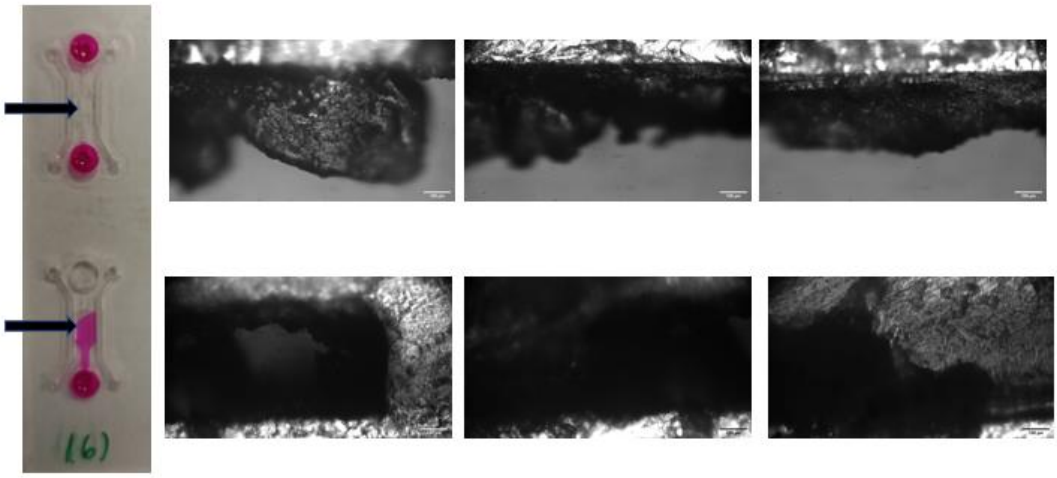

Figure 3.18: Cross-section images (20X magnification) of bonded PMMA (150/400 µm) with 40% ETOH+60% ACE with plasma treatment.

Microscope images of the cross-section of the microfluidic chip bonded with an 80% ETOH+20% ACE mixture are given in Figure 3.19. The height of the side channel is 343 µm, and the central channel is 116 µm for the chip with a retention groove. For the bottom design, the height of the side channel is 385 µm, and the main channel is 137 µm. Increasing ETOH volume solved to clogging problem, as seen in Figure 3.19. In this case, the addition of a retention groove causes a reduction of channels. Using 80% ETOH+20% ACE as a solvent having no retention groove is a better case for fabricating a microfluidic chip.

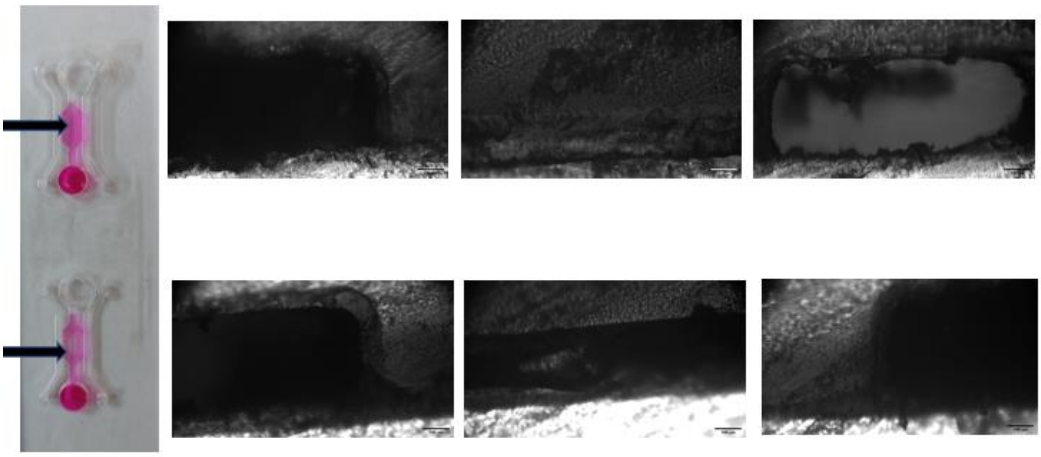

Figure 3.19: Cross-section images (20X magnification) of bonded PMMA (150/400 µm) with 80% ETOH+20% ACE with plasma treatment.

Microscope images of the cross-section of the microfluidic chip bonded with 80% IPA+20% ACE mixture and without plasma treatment are given in Figure 3.20. The height of the side channel is 392 µm, and the central channel is 145 µm for the chip with a retention groove. If the plasma treatment is not used, there can be clogging problems due to wettability being worse than without plasma treatment. In addition, there was no relation between plasma treatment and the height of channels concerning samples bonded with 80% IPA+ 20% ACE mixture with or without plasma treatment.

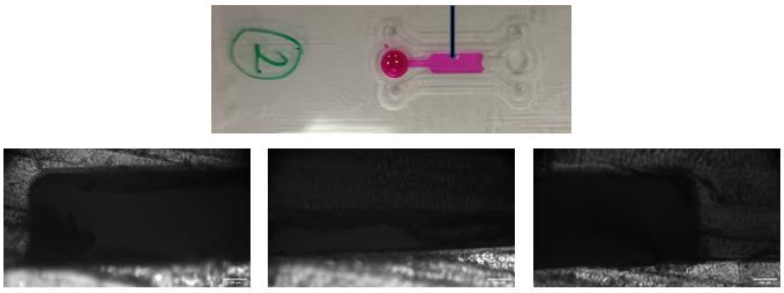

Figure 3.20: Cross-section images (20X magnification) of bonded PMMA (150/400 µm) with 80% IPA+20% ACE without plasma treatment.

Microscope images of the cross-section of the microfluidic chip bonded with 100% ACE and without plasma treatment are given in Figure 3.21. The height of the side channel is 344 µm, and the central channel is 65 µm for the chip with a retention groove. The worst solvent for fabricating microfluidic chips is 100% ACE. Figure 3.21 shows the clogged channels, and some areas are not clogged, but the reduction of the channel has occurred. Before bonding, the height of the side channel was 400 µm, but after the bonding procedure became 357 µm. For the central channel, the reduction ratio is 56%, which is so unwanted case concerning the application. The confinement test shows that the beginning of the channel and other regions were clogged.

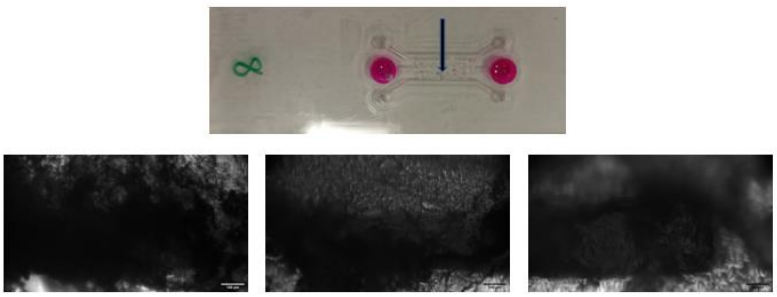

Figure 3.21: Cross-section images (20X magnification) of bonded PMMA (150/400 µm) with 100 % ACE without plasma treatment.

3.4.5 Diffusion Tests

For the design with h=150/400 µm channel height, the diffusion of water was observed using dyed water at no speed. After adding collagen to the central channel, using a micropipette pump from the side channel at continuous rates of 0 dyed water was given. In Figure 3.22, images from the side channel after the start of dyed water (a) t=10 min (b) t=30 min (c) t=60 min are given. If the PDMS chip is compared with the PMMA chip in terms of diffusion test, it is seen that the dyed water diffuses more homogeneously in the PMMA chip.

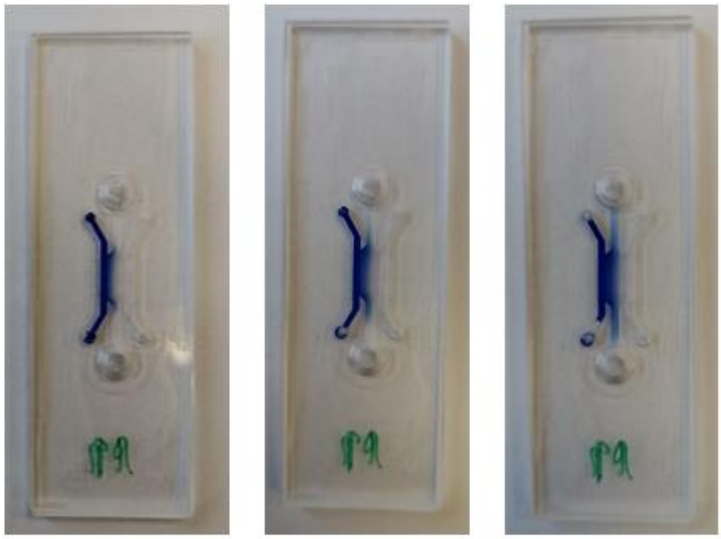

Figure 3.22: Diffusion of dyed water through the hydrogel inside the middle channel when V=0 a) t=10 min b)30 min c) 60 min.

3.4.6 3D Cell Culturing

For cell studies, PMMA was bonded with a mixture of 80% IPA + 20% ACE with plasma treatment by heating at 65°C. Figure 3.23 shows the microscope images of the PMMA chips one week after the collagen was loaded. The images show that the collagen was loaded successfully with microfluidic chips made by PMMA. The next step is creating an appropriate medium for cells.

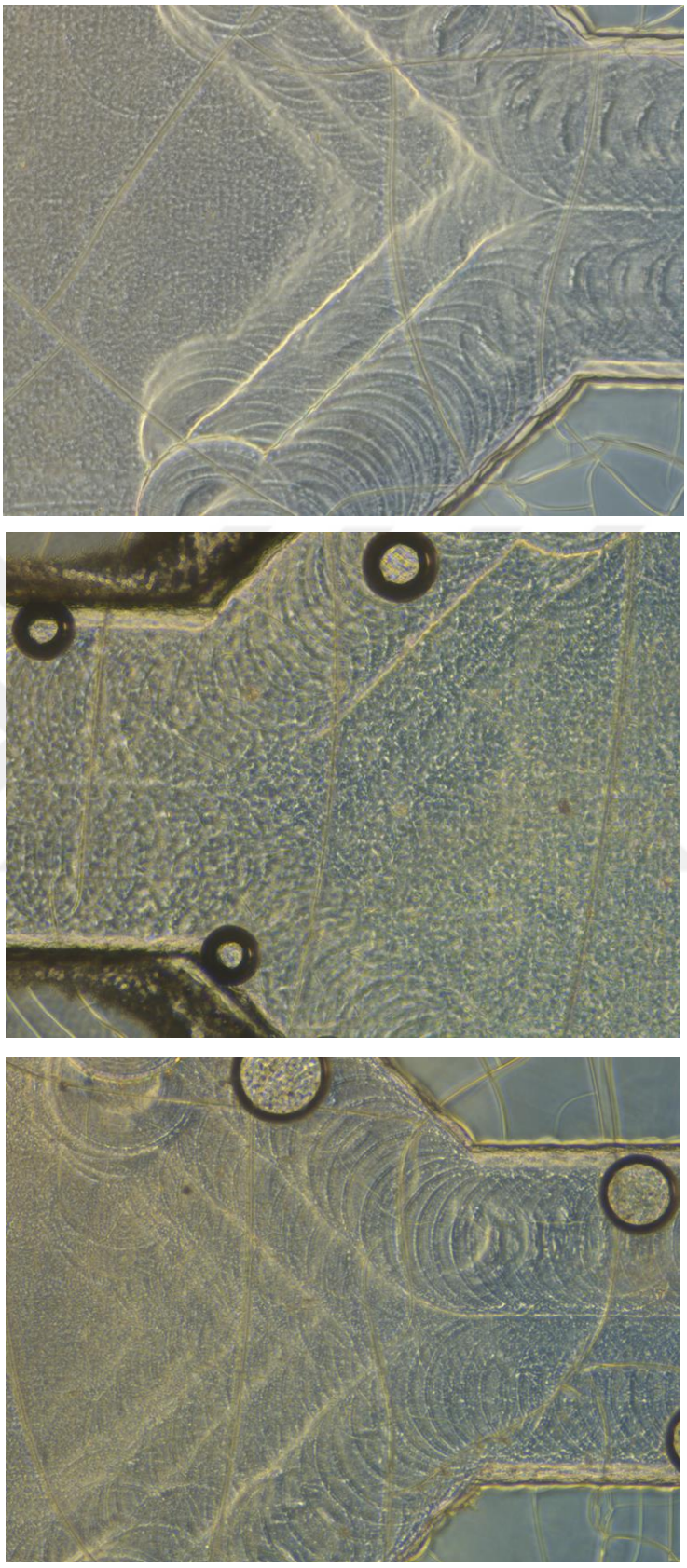

Figure 3.23: The microscope images (10X magnification) of PMMA chips collagen were added one week later.

Initially, the central channel was filled with collagen, and hydrogel formation was accomplished in the incubator as described above. SNU 484 gastric cancer cells were added to the side channel as 20.000 cells per 10 µL volume. The chips were centrifuged at 300 g for 1 minute to enable cell adherence to collagen and entry of cells into the groove.

Figure 3.24 shows the cell seeding steps after collagen filling. There was no cleaning step for this microfluidic chip. Therefore, it was observed that the cells died three days after they were seeded. Cells were presumed dead due to IPA or ACE remaining in the channels during PMMA bonding. A cleaning step was added to the bonding procedure to confirm this assumption. Images after this cleaning step are presented in Figure 3.25. Cells were seen alive after cell seeding on this microfluidic chip, and these images show that the added cleaning step worked. These microfluidic chips fabricated by this method are ready for 3D cell studies.

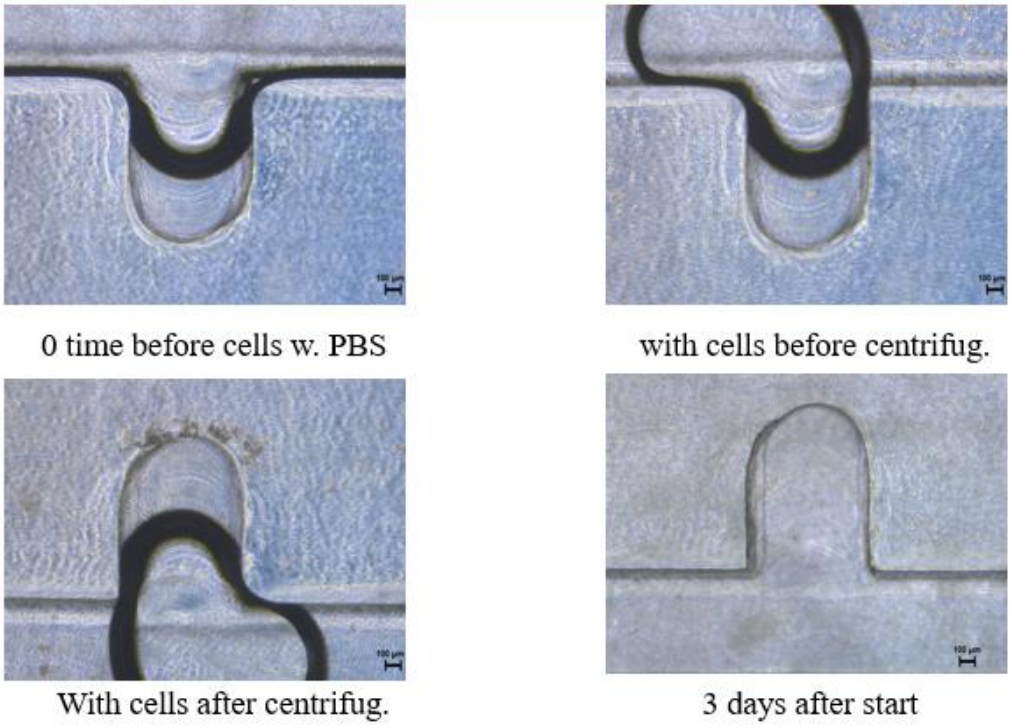

Figure 3.24: Cell culture images (10X magnification) with time before the cleaning step.

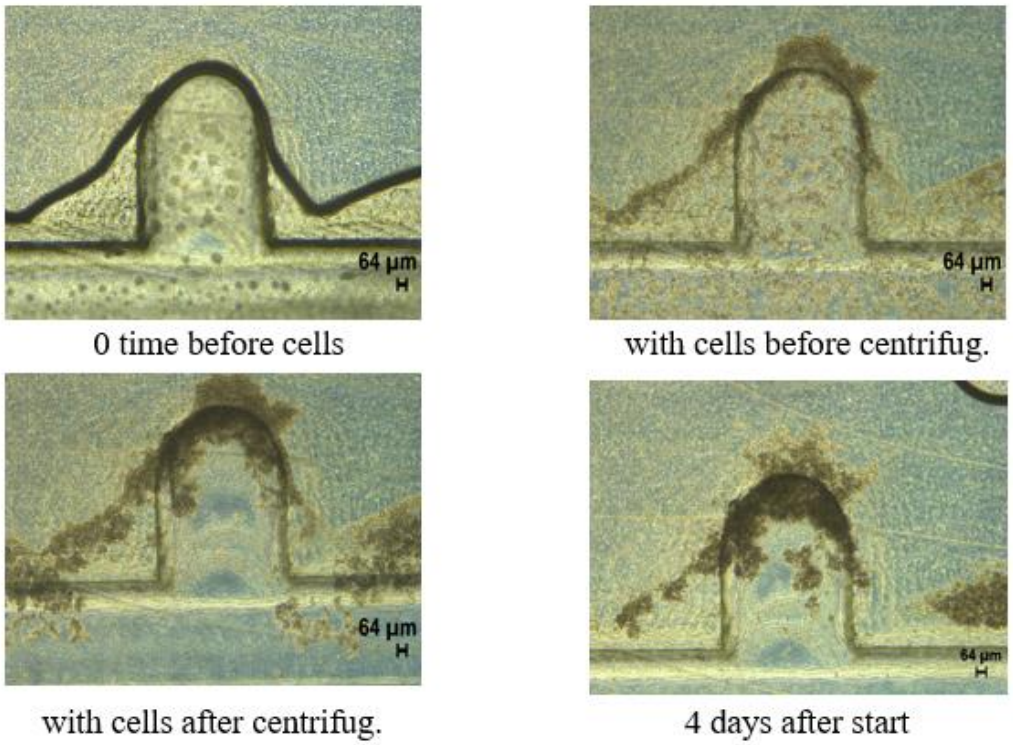

Figure 3.25: Cell culture images (10X magnification) using SN 484 cells with time after the cleaning step.

3.5 Discussion

We fabricated PMMA microfluidic chips in this chapter using the solvent bonding technique. We chose the micro-milling technique for processing the PMMA. This technique does not need the master mold; the main advantage is the flexibility of the design. We processed precisely the PMMA by using CNC according to profilometer results. After preparing the mold according to the Hildebrandt parameter, we decided on the optimum solvent mixtures. We tested ETOH+ACE and IPA+ACE mixtures with different ratios. Firstly, we calculated the bonding coverage for each mixture. The bonding coverage results show that high ratios of acetone and ethanol increase the bonding coverage. But the microscope images of the bonded PMMA show that acetone causes cracks, and according to cross-section images, we show that acetone causes clogging problems. We found that ethanol and isopropyl alcohol are not harmful to the bonded surface. Also, adding plasma treatment to the procedure decreases the surface cracks. In order to compare the bonding strength with different solvents, temperatures, and plasma treatment, we did tensile strength tests. According to bonding strength experiments, we demonstrated that PMMA was bonded irreversibly. We bonded PMMA at room temperature, and the result shows that at least 60% ACE mixtures can be bonded

at room temperature. Since the Hildebrandt parameter of ACE and IPA is so close, this result was expected. We fabricated PMMA microfluidic chips with different mixtures and cut the chip for examining cross-section images. In addition to these experiments, we did confinement tests by loading dye water into the central channel. Cross-section images show that 80% IPA+20% ACE and 80% ETOH+20% do not cause a clogging problem, and this mixture can be used for fabricating PMMA-based microfluidic chips. There were clogging problems with the mixtures having at least %60 ACE, as expected. Also, adding a retention groove around the design improves the bonding due to the confinement of the solvent. According to diffusion tests, we show that when the central channel was loaded with collagen, the dye water that we gave from the side channel diffused homogeneously. We chose 80% IPA+20% ACE mixture at 65°C for 10 min, at room temperature for 5 min with plasma treatment for cell experiments. After the PMMA-based microfluidic chip was fabricated, we were able to culture cells after loading collagen. As a result, we successfully produced a PMMA-based microfluidic chip using solvent bonding for cell culturing. For future studies, these microfluidic chips can be used in various cell applications.

Chapter 4

CONCLUSION

In Chapter 2, we fabricated a suitable PDMS-based microfluidic chip for cell experiments with an easy and inexpensive method. The molds were prepared by cutting tapes with a digital craft cutter. However, since the resolution of this device was lower than the groove structures we wanted to add to the design, we changed the mold preparation method to CNC. Profilometer results show that we can produce the molds we use very precisely. There is a confinement problem design with four 300-diameter grooves. The number of grooves was reduced, and the diameter was increased to solve this problem. The design was updated to have three grooves with 600 µm diameters, and the confinement problem was solved. PDMS-based microfluidic chips were used in two different cell applications. The first was human aortic primary vascular smooth muscle cell culturing in the collagen gel. The other study investigates the response of HUVEC cells to the hydrogel in the microfluidic chips to TNF-α. Images taken with the confocal microscope show that the appropriate environment for cell studies has been successfully fabricated.

In Chapter 3, we aimed to fabricate PMMA microfluidic chips that can work with cells by changing parameters such as temperature, solvent, plasma treatment, and retention groove. According to the profilometer measurement results, it was processed using PMMA CNC with very high resolution. One of the quality bonding parameters is bonding coverage. Bonding coverage experiments with different percentages of ETOH, IPA, and ACE generally increase plasma bonding coverage. In addition, as the amount of acetone in the mixture increases, the bonding coverage increases. In experiments performed at room temperature and using an oven at 65°C, bonding was observed in cases where there was at least 60% ACE in the solvent. These results showed that PMMA bonded even at room temperature when using ACE, but this caused the clogging problem in microfluidic chip fabrication. Therefore, attempts were made to find a solvent mixture with strong bonding and no damage to the channels. Combinations of 40% ETOH+60% ACE, 80% IPA +20% ACE, and 80% ETOH+20% ACE were used in these trials. Cross-section images show that the clogging problem is seen in the channels as the amount of ACE increases. In addition, the retention groove improved bonding by allowing these

volatile solvents to hold more, as expected. According to the confinement tests of microfluidic chips produced with 80% IPA + 20% ACE mixture with the same parameters except for plasma treatment, the problem of clogging in the channels arose when plasma was not applied. The reason is that the plasma applied surface is too hydrophilic, so the contact angles of PMMA after plasma were measured. Based on the cross-section images, the solvent mixture used in the cell study was chosen as 80% IPA + 20% ACE. Collagen filling of PMMA microfluidic chips produced by this method has been successful. The microscope images show that the SNU 484 cancer cells placed into the side channel after the collagen filling has attached and are alive after 4 days of culture. The solvent bonding technique successfully fabricated a PMMA microfluidic chip that can also be used for other cell studies.

BIBLIOGRAPHY

[Attia et al., 2009] Attia, U. M., Marson, S., & Alcock, J. R. (2009). Micro-injection moulding of polymer microfluidic devices. In Microfluidics and Nanofluidics (Vol. 7, Issue 1, pp. 1–28). Springer Science and Business Media LLC. https://doi.org/10.1007/s10404-009-0421-x

[Bamshad et al., 2016] Bamshad, A., Nikfarjam, A., & Khaleghi, H. (2016). A new simple and fast thermally-solvent assisted method to bond PMMA–PMMA in micro-fluidics devices. In Journal of Micromechanics and Microengineering (Vol. 26, Issue 6, p. 065017). IOP Publishing. https://doi.org/10.1088/0960-1317/26/6/065017

[Bruijns et al., 2019] Bruijns, B., Veciana, A., Tiggelaar, R., & Gardeniers, H. (2019). Cyclic Olefin Copolymer Microfluidic Devices for Forensic Applications. In Biosensors (Vol. 9, Issue 3, p. 85). MDPI AG. https://doi.org/10.3390/bios9030085

[Brydson, 1999] Brydson J (1999) Plastic materials. Butterworth-Heinemann, Oxford

[Cate and Adkins, 2014] Cate, D. M., Adkins, J. A., Mettakoonpitak, J., & Henry, C. S. (2014). Recent Developments in Paper-Based Microfluidic Devices. In Analytical Chemistry (Vol. 87, Issue 1, pp. 19–41). American Chemical Society (ACS). https://doi.org/10.1021/ac503968p

[Chen and Duong,2016] Chen, P.-C., & Duong, L. H. (2016). Novel solvent bonding method for thermoplastic microfluidic chips. In Sensors and Actuators B: Chemical (Vol. 237, pp. 556–562). Elsevier BV. https://doi.org/10.1016/j.snb.2016.06.135

[Chen et al., 2016] Chen, P.-C., Liu, Y.-M., & Chou, H.-C. (2016). An adhesive bonding method with microfabricating micro pillars to prevent clogging in a microchannel. In Journal of Micromechanics and Microengineering (Vol. 26, Issue 4, p. 045003). IOP Publishing. https://doi.org/10.1088/0960-1317/26/4/045003

Bibliography

[Coskun et al., 2022] Coskun, U. C., Kus, F., Rehman, A. U., Morova, B., Gulle, M., Baser, H., Kul, D., Kiraz, A., Baysal, K., & Erten, A. (2022). An Easy-to-Fabricate Microfluidic Shallow Trench Induced Three-Dimensional Cell Culturing and Imaging (STICI3D) Platform. In ACS Omega (Vol. 7, Issue 10, pp. 8281–8293). American Chemical Society (ACS). https://doi.org/10.1021/acsomega.1c05118

[Elliott and Yuan,2011] Elliott, N. T., & Yuan, F. (2011). A Review of Three-Dimensional In Vitro Tissue Models for Drug Discovery and Transport Studies. Journal of Pharmaceutical Sciences, 100(1), 59-74. https://doi.org/10.1002/jps.22257

[Faghih and Sharp,2018] Faghih, M. M., & Sharp, M. K. (2018). Solvent-based bonding of PMMA–PMMA for microfluidic applications. In Microsystem Technologies (Vol. 25, Issue 9, pp. 3547–3558). Springer Science and Business Media LLC. https://doi.org/10.1007/s00542-018-4266-7

[Giri and Tsao, 2022] Giri, K., & Tsao, C.-W. (2022). Recent Advances in Thermoplastic Microfluidic Bonding. In Micromachines (Vol. 13, Issue 3, p. 486). MDPI AG. https://doi.org/10.3390/mi13030486

[Halldorsson et al., 2015] Halldorsson, S., Lucumi, E., Gómez-Sjöberg, R., & Fleming, R. M. T. (2015). Advantages and challenges of microfluidic cell culture in polydimethylsiloxane devices. In Biosensors and Bioelectronics (Vol. 63, pp. 218–231). Elsevier BV. https://doi.org/10.1016/j.bios.2014.07.029

[Hildebrandt and Scott, 1949] Hildebrandt J, Scott R (1949) The solubility of non-electrolytes.Reinhold, New York

[Hosic et al., 2015] Hosic, S., Murthy, S. K., & Koppes, A. N. (2015). Microfluidic Sample Preparation for Single Cell Analysis. In Analytical Chemistry (Vol. 88, Issue 1, pp. 354–380). American Chemical Society (ACS). https://doi.org/10.1021/acs.analchem.5b04077

Bibliography

[Jena and Yue, 2012] Jena, R. K., & Yue, C. Y. (2012). Cyclic olefin copolymer based microfluidic devices for biochip applications: Ultraviolet surface grafting using 2-methacryloyloxyethyl phosphorylcholine. In Biomicrofluidics (Vol. 6, Issue 1, p. 012822). AIP Publishing. https://doi.org/10.1063/1.3682098

[Kamei et al., 2015] Kamei, K., Mashimo, Y., Koyama, Y., Fockenberg, C., Nakashima, M., Nakajima, M., Li, J., & Chen, Y. (2015). 3D printing of soft lithography mold for rapid production of polydimethylsiloxane-based microfluidic devices for cell stimulation with concentration gradients. In Biomedical Microdevices (Vol. 17, Issue 2). Springer Science and Business Media LLC. https://doi.org/10.1007/s10544-015-9928-y

[Karimi et al., 2016] Karimi, M., Bahrami, S., Mirshekari, H., Basri, S. M. M., Nik, A. B., Aref, A. R., Akbari, M., & Hamblin, M. R. (2016). Microfluidic systems for stem cell-based neural tissue engineering. In Lab on a Chip (Vol. 16, Issue 14, pp. 2551–2571). Royal Society of Chemistry (RSC). https://doi.org/10.1039/c6lc00489j

[Kelly and Woolley,2003] Kelly, R. T., & Woolley, A. T. (2003). Thermal Bonding of Polymeric Capillary Electrophoresis Microdevices in Water. In Analytical Chemistry (Vol. 75, Issue 8, pp. 1941–1945). American Chemical Society (ACS). https://doi.org/10.1021/ac0262964

[Lai et al., 2004] Lai, S., Cao, X., & Lee, L. J. (2004). A Packaging Technique for Polymer Microfluidic Platforms. In Analytical Chemistry (Vol. 76, Issue 4, pp. 1175–1183). American Chemical Society (ACS). https://doi.org/10.1021/ac034990t

[Le et al., 2021] Le, N. X. T., Trinh, K. T. L., & Lee, N. Y. (2021). Poly (acrylic acid) as an adhesion promoter for UV-assisted thermoplastic bonding: Application for the in vitro construction of human blood vessels. In Materials Science and Engineering: C (Vol. 122, p. 111874). Elsevier BV. https://doi.org/10.1016/j.msec.2021.111874

[Lee et al., 2003] Lee, J. N., Park, C., & Whitesides, G. M. (2003). Solvent Compatibility of Poly(dimethylsiloxane)-Based Microfluidic Devices. In Analytical Chemistry (Vol.

75, Issue 23, pp. 6544–6554). American Chemical Society (ACS). https://doi.org/10.1021/ac0346712

[Lei et al., 2017] Lei, K. F., Chang, C.-H., & Chen, M.-J. (2017). Paper/PMMA Hybrid 3D Cell Culture Microfluidic Platform for the Study of Cellular Crosstalk. In ACS Applied Materials & Interfaces (Vol. 9, Issue 15, pp. 13092–13101). American Chemical Society (ACS). https://doi.org/10.1021/acsami.7b03021

[Li et al., 2012] Li, X. (James), Valadez, A. V., Zuo, P., & Nie, Z. (2012). Microfluidic 3D cell culture: potential application for tissue-based bioassays. In Bioanalysis (Vol. 4, Issue 12, pp. 1509–1525). Future Science Ltd. https://doi.org/10.4155/bio.12.133

[Li et al., 2016] Li, Y., Chen, D., Zhang, Y., Liu, C., Chen, P., Wang, Y., Feng, X., Du, W., & Liu, B.-F. (2016). High-throughput single cell multidrug resistance analysis with multifunctional gradients-customizing microfluidic device. In Sensors and Actuators B: Chemical (Vol. 225, pp. 563–571). Elsevier BV. https://doi.org/10.1016/j.snb.2015.11.097

[Liu and Crooks, 2011] Liu, H., & Crooks, R. M. (2011). Three-Dimensional Paper Microfluidic Devices Assembled Using the Principles of Origami. In Journal of the American Chemical Society (Vol. 133, Issue 44, pp. 17564–17566). American Chemical Society (ACS). https://doi.org/10.1021/ja2071779

[Liu et al., 2009] Liu, J., Qiao, H., Liu, C., Xu, Z., Li, Y., & Wang, L. (2009). Plasma assisted thermal bonding for PMMA microfluidic chips with integrated metal microelectrodes. In Sensors and Actuators B: Chemical (Vol. 141, Issue 2, pp. 646–651). Elsevier BV. https://doi.org/10.1016/j.snb.2009.07.032

Material Properties of Polystyrene and Poly (methyl methacrylate) (PMMA) Microspheres. Available online: https://www.bangslabs.com/material-properties-polystyrene-and-polymethyl-methacrylate-pmma-microspheres (accessed on 25 February 2022)

Bibliography

[McDonald et al., 2000] McDonald, J. C., Duffy, D. C., Anderson, J. R., Chiu, D. T., Wu, H., Schueller, O. J. A., & Whitesides, G. M. (2000). Fabrication of microfluidic systems in poly(dimethylsiloxane). In Electrophoresis (Vol. 21, Issue 1, pp. 27–40). Wiley. https://doi.org/10.1002/(sici)1522-2683(20000101)21:1<27::aid-elps27>3.0.co;2-c

[Mekaru,2018] Mekaru, H. (2018). Thermal and ultrasonic bonding between planar polyethylene terephthalate, acrylonitrile butadiene styrene, and polycarbonate substrates. In International Journal of Adhesion and Adhesives (Vol. 84, pp. 394–405). Elsevier BV. https://doi.org/10.1016/j.ijadhadh.2018.05.001

[Miyazaki et al., 2017] Miyazaki, K., Hashimoto, K., Sato, M., Watanabe, M., Tomikawa, N., Kanno, S., Kawasaki, Y., Momoi, N., & Hosoya, M. (2017). Establishment of a method for evaluating endothelial cell injury by TNF-α in vitro for clarifying the pathophysiology of virus-associated acute encephalopathy. In Pediatric Research (Vol. 81, Issue 6, pp. 942–947). Springer Science and Business Media LLC. https://doi.org/10.1038/pr.2017.28

[Nguyen et al., 2019] Nguyen, T., Anh Ngo, T., Duong Bang, D., & Wolff, A. (2019). Optimising the supercritical angle fluorescence structures in polymer microfluidic biochips for highly sensitive pathogen detection: a case study on Escherichia coli. In Lab on a Chip (Vol. 19, Issue 22, pp. 3825–3833). Royal Society of Chemistry (RSC). https://doi.org/10.1039/c9lc00888h

[Nishat et al., 2021] Nishat, S., Jafry, A. T., Martinez, A. W., & Awan, F. R. (2021). Paper-based microfluidics: Simplified fabrication and assay methods. In Sensors and Actuators B: Chemical (Vol. 336, p. 129681). Elsevier BV. https://doi.org/10.1016/j.snb.2021.129681

[Roth and Drummer, 2021] Roth, B., & Drummer, D. (2021). Pressure Equilibrium Time of a Cyclic-Olefin Copolymer. In Polymers (Vol. 13, Issue 14, p. 2309). MDPI AG. https://doi.org/10.3390/polym13142309

Bibliography

[Roy et al., 2016] Roy, E., Pallandre, A., Zribi, B., Horny, M.-C., Delapierre, F. D., Cattoni, A., Gamby, J., & Haghiri-Gosnet, A.-M. (2016). Overview of Materials for Microfluidic Applications. In Advances in Microfluidics - New Applications in Biology, Energy, and Materials Sciences. InTech. https://doi.org/10.5772/65773

[Sackmann et al., 2014] Sackmann, E. K., Fulton, A. L., & Beebe, D. J. (2014). The present and future role of microfluidics in biomedical research. In Nature (Vol. 507, Issue 7491, pp. 181–189). Springer Science and Business Media LLC. https://doi.org/10.1038/nature13118

[Shakeri et al., 2021] Shakeri, A., Khan, S., & Didar, T. F. (2021). Conventional and emerging strategies for the fabrication and functionalization of PDMS-based microfluidic devices. In Lab on a Chip (Vol. 21, Issue 16, pp. 3053–3075). Royal Society of Chemistry (RSC). https://doi.org/10.1039/d1lc00288k

[Shakeri et al., 2022] Shakeri, A., Khan, S., Jarad, N. A., & Didar, T. F. (2022). The Fabrication and Bonding of Thermoplastic Microfluidics: A Review. In Materials (Vol. 15, Issue 18, p. 6478). MDPI AG. https://doi.org/10.3390/ma15186478

[Sia and Whitesides, 2003] Sia, S. K., & Whitesides, G. M. (2003). Microfluidic devices fabricated in Poly(dimethylsiloxane) for biological studies. In ELECTROPHORESIS (Vol. 24, Issue 21, pp. 3563–3576). Wiley. https://doi.org/10.1002/elps.200305584

[Spurgeon et al., 2008] Spurgeon, S. L., Jones, R. C., & Ramakrishnan, R. (2008). High Throughput Gene Expression Measurement with Real Time PCR in a Microfluidic Dynamic Array. In C. Seoighe (Ed.), PLoS ONE (Vol. 3, Issue 2, p. e1662). Public Library of Science (PLoS). https://doi.org/10.1371/journal.pone.0001662

[Su et al., 2019] Su, S., Jing, G., Zhang, M., Liu, B., Zhu, X., Wang, B., Fu, M., Zhu, L., Cheng, J., & Guo, Y. (2019). One-step bonding and hydrophobic surface modification method for rapid fabrication of polycarbonate-based droplet microfluidic chips. In Sensors and Actuators B: Chemical (Vol. 282, pp. 60–68). Elsevier BV. https://doi.org/10.1016/j.snb.2018.11.035

[Tanyeri and Tay, 2018] Tanyeri, M., & Tay, S. (2018). Viable cell culture in PDMS-based microfluidic devices. In Methods in Cell Biology (pp. 3–33). Elsevier. https://doi.org/10.1016/bs.mcb.2018.09.007

[Terry et al., 1979] Terry, S. C., Jerman, J. H., & Angell, J. B. (1979). A gas chromatographic air analyzer fabricated on a silicon wafer. In IEEE Transactions on Electron Devices (Vol. 26, Issue 12, pp. 1880–1886). Institute of Electrical and Electronics Engineers (IEEE). https://doi.org/10.1109/t-ed.1979.19791

[Theobald et al., 2017] Theobald, J., Ghanem, A., Wallisch, P., Banaeiyan, A. A., Andrade-Navarro, M. A., Taškova, K., Haltmeier, M., Kurtz, A., Becker, H., Reuter, S., Mrowka, R., Cheng, X., & Wölfl, S. (2017). Liver-Kidney-on-Chip to Study Toxicity of Drug Metabolites. In ACS Biomaterials Science & Engineering (Vol. 4, Issue 1, pp. 78–89). American Chemical Society (ACS). https://doi.org/10.1021/acsbiomaterials.7b00417

[Torino et al., 2018] Torino, S., Corrado, B., Iodice, M., & Coppola, G. (2018). PDMS-Based Microfluidic Devices for Cell Culture. In Inventions (Vol. 3, Issue 3, p. 65). MDPI AG. https://doi.org/10.3390/inventions3030065

[Trinh et al., 2021] Trinh, K. T. L., Chae, W. R., & Lee, N. Y. (2021). Pressure-Free Assembling of Poly (methyl methacrylate) Microdevices via Microwave-Assisted Solvent Bonding and Its Biomedical Applications. In Biosensors (Vol. 11, Issue 12, p. 526). MDPI AG. https://doi.org/10.3390/bios11120526

[Trinh et al., 2022] Trinh, K. T. L., Thai, D. A., & Lee, N. Y. (2022). Bonding Strategies for Thermoplastics Applicable for Bioanalysis and Diagnostics. In Micromachines (Vol. 13, Issue 9, p. 1503). MDPI AG. https://doi.org/10.3390/mi13091503

[Tsao and DeVoee, 2008] Tsao, C.-W., & DeVoe, D. L. (2008). Bonding of thermoplastic polymer microfluidics. In Microfluidics and Nanofluidics (Vol. 6, Issue 1, pp. 1–16). Springer Science and Business Media LLC. https://doi.org/10.1007/s10404-008-0361-x

[Tsao et al., 2022] Tsao, C.-W., Chang, C.-Y., & Chien, P.-Y. (2022). Microwave-Assisted Solvent Bonding for Polymethyl Methacrylate Microfluidic Device. In Micromachines (Vol. 13, Issue 7, p. 1131). MDPI AG. https://doi.org/10.3390/mi13071131

[Wan et al., 2015] Wan, A. M. D., Sadri, A., & Young, E. W. K. (2015). Liquid phase solvent bonding of plastic microfluidic devices assisted by retention grooves. In Lab on a Chip (Vol. 15, Issue 18, pp. 3785–3792). Royal Society of Chemistry (RSC). https://doi.org/10.1039/c5lc00729a

[Wan et al., 2017] Wan, A. M. D., Moore, T. A., & Young, E. W. K. (2017). Solvent Bonding for Fabrication of PMMA and COP Microfluidic Devices. In Journal of Visualized Experiments (Issue 119). MyJove Corporation. https://doi.org/10.3791/55175

[Wang et al., 2018] Wang, X., Sun, Q., & Pei, J. (2018). Microfluidic-Based 3D Engineered Microvascular Networks and Their Applications in Vascularized Microtumor Models. In Micromachines (Vol. 9, Issue 10, p. 493). MDPI AG. https://doi.org/10.3390/mi9100493

[Xu et al., 2013] Xu, T., Yue, W., Li, C.-W., Yao, X., & Yang, M. (2013). Microfluidics study of intracellular calcium response to mechanical stimulation on single suspension cells. In Lab on a Chip (Vol. 13, Issue 6, p. 1060). Royal Society of Chemistry (RSC). https://doi.org/10.1039/c3lc40880a

[Xue et al., 2020] Xue, B., Geng, Y., Yan, Y., Ma, G., Wang, D., & He, Y. (2020). Rapid prototyping of microfluidic chip with burr-free PMMA microchannel fabricated by revolving tip-based micro-cutting. In Journal of Materials Processing Technology (Vol. 277, p. 116468). Elsevier BV. https://doi.org/10.1016/j.jmatprotec.2019.116468